“BIOPHYSICAL AND BIOCHEMICAL CHARACTERIZATION OF PROTEINS ENCODED BY MICRO-EXON GENES (MEGs) 3.3 AND 3.4 FROM *SCHISTOSOMA MANSONI*”

“CARACTERIZAÇÃO BIOFÍSICA E BIOQUÍMICA DAS PROTEÍNAS CODIFICADAS PELOS MICRO-EXON GENES (MEGs) 3.3 E 3.4 DO *SCHISTOSSOMA MANSONI*”

REMY GABRIEL CABEZUDO COBOS

STATE UNIVERSITY OF NORTHERN RIO DE JANEIRO DARCY RIBEIRO

UNIVERSIDADE ESTADUAL DO NORTE FLUMINENSE DARCY RIBEIRO

CAMPOS DOS GOYTACAZES – RJ

FEBRUARY, 2026

“BIOPHYSICAL AND BIOCHEMICAL CHARACTERIZATION OF PROTEINS ENCODED BY MICRO-EXON GENES (MEGs) 3.3 AND 3.4 FROM *SCHISTOSOMA MANSONI*”

“CARACTERIZAÇÃO BIOFÍSICA E BIOQUÍMICA DAS PROTEÍNAS CODIFICADAS PELOS MICRO-EXON GENES (MEGs) 3.3 E 3.4 DO *SCHISTOSSOMA MANSONI*”

REMY GABRIEL CABEZUDO COBOS

Thesis presented to the Center for Biosciences and Biotechnology at the State University of Norther Rio de Janeiro Darcy Ribeiro, as part of the requirements for obtaining the title of Master in Bioscience and Biotechnology.

ADVISOR: Prof. Dr. Ana Eliza Zeraik

STATE UNIVERSITY OF NORTHERN RIO DE JANEIRO DARCY RIBEIRO

UNIVERSIDADE ESTADUAL DO NORTE FLUMINENSE DARCY RIBEIRO

CAMPOS DOS GOYTACAZES – RJ

FEBRUARY, 2026

FICHA CATALOGRÁFICA
UENF - Bibliotecas
Elaborada com os dados fornecidos pelo autor.

C657 Cobos, Remy Gabriel Cabezudo.

"Caracterização Biofísica e Bioquímica das proteínas codificadas pelos Micro-Exon Genes (MEGs) 3.3 e 3.4 do *Schistosoma mansoni*". / Remy Gabriel Cabezudo Cobos. - Campos dos Goytacazes, RJ, 2026.

78 f. : il.
Inclui bibliografia.

Dissertação (Mestrado em Biociências e Biotecnologia) - Universidade Estadual do Norte Fluminense Darcy Ribeiro, Centro de Biociências e Biotecnologia, 2026.
Orientadora: Ana Eliza Zeraik.

1. *Schistosoma mansoni*. 2. Micro-exon gene. 3. Protein characterization. I. Universidade Estadual do Norte Fluminense Darcy Ribeiro. II. Título.

CDD - 570

“BIOPHYSICAL AND BIOCHEMICAL CHARACTERIZATION OF PROTEINS ENCODED BY MICRO-EXON GENES (MEGs) 3.3 AND 3.4 FROM *SCHISTOSOMA MANSONI*”

REMY GABRIEL CABEZUDO COBOS

Thesis presented to the Center for Biosciences and Biotechnology at the State University of Northern Rio de Janeiro Darcy Ribeiro, as part of the requirements for obtaining the title of Master in Biosciences and Biotechnology.

Approved on February 23, 2026.

Examination committee:

Documento assinado digitalmente
gov.br
ANDRE DE OLIVEIRA CARVALHO
Data: 29/04/2026 11:23:28-0300
Verifique em https://validar.iti.gov.br

Prof. Dr. André de Oliveira Carvalho

(Ph.D. in Biosciences and Biotechnology)-LFBM/UENF

Documento assinado digitalmente
gov.br
ANTONIO JESUS DORIGHETTO COGO
Data: 28/04/2026 17:23:19-0300
Verifique em https://validar.iti.gov.br

Prof. Dr. Antônio Jesus Dorighetto Cogo

(Ph. D. in Biosciences and Biotechnology)-LBCT/UENF

Documento assinado digitalmente
gov.br
ITALO AUGUSTO CAVINI
Data: 27/04/2026 17:40:52-0300
Verifique em https://validar.iti.gov.br

Prof. Dr. Ítalo Augusto Cavini

(Ph. D. in Biomolecular Applied Physics)-FCFRP-USP

Documento assinado digitalmente
gov.br
ANA ELIZA ZERAIK
Data: 27/04/2026 16:36:49-0300
Verifique em https://validar.iti.gov.br

Prof. Dr. Ana Eliza Zeraik

(Ph. D. in Biomolecular Applied Physics)-LQFPP/UENF

Dedicatory

"*I see now that the circumstances of one´s birth are irrelevant; it is what you do with the gift of life that determines who you are"*

-Mewtwo

I dedicated this conquest to my entire family, who gave me every opportunity possible and encouraged me to keep growing.

Acknowledgments

I would like to thank my family for their constant support in my development, to my father Remy Orlando and my mother Charito, who have strived every day to raise and educate me and make me the person I am today, trusting in all the decisions I take and supporting me despite the distance on the loneliest and most difficult days. Without them, I would not be where I am today. Thank you for making me feel fortunate to have such wonderful parents. Thank you infinitely.

To Professor Dr Ana Eliza Zeraik, for giving me the opportunity to be part of her research group as a foreign student, and for supporting me from the beginning to the end of my master´s degree with valuable advice, helping me to develop my critical thinking, as well as serving as an example for improving my qualities as a researcher.

To my friends and colleagues from the Molecular Biochemistry and Biophysics group at UENF, who helped me to get started in this new area of study and enabled me to share and collaborate during the last two years, especially Lorran, Marcos and Yhony, for their great support during these two years of fail and successful experiments.

To the professors of the Centro de Biociências e Biotecnologia (CBB) at UENF, especially those who are part of the Laboratorio de Química e Função de Proteínas e Peptídeos (LQFPP) and Laboratorio de Fisiologia e Bioquímica de Microorganismos (LFBM), for joining in and assisting in my professional training and providing important knowledge from their areas of expertise. I would also like to thank the technical staff at the laboratory for their assistance.

To the administrative staff and faculty members of the Programa de Pós-Graduação em Biociências e Biotecnologia for their support and guiadence during the master´s degree.

Finally, I would like to express my sincere thanks to the Universidade Estadual do Norte Fluminense Darcy Ribeiro-UENF for the great opportunity given to me. *This work was supported by Fundação Carlos Chagas Filho de Amparo à Pesquisa do Estudo do Rio de Janeiro (FAPERJ E-26/200.177/2023, E-26/210.094/2022, #E-26/211.860/2021, Conselho Nacional de Desenvolvimento Científico e Tecnológico (CNPq 420049/2023-1), Coordeenação de Aperfeiçoamento de Pessoal de Nível Superior (CAPES)-Finance code 001 and this research was also conducted using*

infraestructure funded by Finep under the FINEP/MCTI/FNDCT/PROINFRA2021 program (Agreement No. 0.1.22.0442.00).

TABLE OF CONTENTS

ABBREVIATIONS

$ABTS^+$	2,2'-azinobis-(3-ethylbenzothiazoline-6-sulfonate)
CD	Circular Dichroism
DLS	Dynamic Light Scattering
DSS	Disuccinimidyl suberate
DTT	Dithiothreitol
HEPES	N-2-hydroxyethylpiperazine-N-2-ethanesulfonic acid
IPSE	Interleukin-4-inducing principle of *S. mansoni* eggs
IPTG	Isopropyl β-D-1-thiogalactopyranoside
LB	Luria Bertani
MEGs	Micro-Exon Genes
MWC	Molecular Weight Cutoff
NCBI	National Center for Biotechnology Information
Ni-NTA	Nickel-Nitrilotriacetic Acid
nm	nanometre
OD	Optical Density
pI	Theoretical isoelectric point
pLDDT	predicted local distance difference test
S. mansoni	*Schistosoma mansoni*
SDS	Sodium Dodecyl Sulphate
SDS-PAGE	Sodium Dodecyl Sulphated-Polyacrylamide gel electrophoresis
SEC	Size Exclusion Chromatography
UTR	Untranslated regions
UV	Ultraviolet

LIST OF FIGURES

Descriptions

LIST OF TABLES

Descriptions

ABSTRACT

Schistosoma mansoni is an endemic disease and a significant global health concern, with widespread distribution across South America, Africa and Asia, resulting in approximately 200,000 deaths annually. In Brazil, around 2.8 % of the population is at risk of infection by *Schistosoma mansoni*, the etiological agent of the disease. Although praziquantel is the primary drug used for treatment, its continued use raises concerns about the emergence of drug-resistant strains. The publication of the *S. mansoni* genome revealed a group of proteins encoded by Micro-Exon Genes (MEGs), characterized by multiple isoforms and highly conserved small exons that allow for alternative splicing. Among them, MEG3.3 is notably upregulated in eggs and MEG3.4 in the esophageal gland of *S. mansoni*. Such expression patterns indicate that both proteins, by being present at the parasite-host interface, may play a relevant role in modulating this interaction and represent potential therapeutic targets. This study investigates the MEG3.3 and MEG3.4 proteins through recombinant expression, purification, biophysical characterization, and analysis of theirs interaction with Zn^{2+} and Cu^{2+}. The results revealed that MEG3.4 undergoes conformational changes in its secondary structure induced by Zn^{2+}. For MEG3.3, as also observed for MEG3.4, the circular dichroism spectrum revealed conformational changes in the secondary structure induced by Zn^{2+} and Cu^{2+} titration. Dynamic Light Scattering (DLS) and chemical crosslinking assays demonstrated the formation of oligomers under the same conditions, corroborating the critical participation of the thiol groups as coordination sites for the Zn^{2+} and Cu^{2+} binding. Similarly to metallothioneins, MEG3.3 exhibited high free-radical scavenging activity in the $ABTS^{+}$ assays. These findings deepen the understanding of MEG-encoded proteins, which remain poorly characterized, revealing structural and functional properties previously unknown. In addition, these results may guide the future development of therapeutic strategies targeting MEG proteins as key factors involved in the survival of *Schistosoma mansoni.*

RESUMO

A esquistossomose é uma doença endêmica e uma preocupação significativa para a saúde global, com ampla distribuição na América do Sul e na África, resultando em aproximadamente 200.000 mortes por ano. No Brasil, cerca de 2,8% da população está em risco de infecção pelo *Schistosoma mansoni*, o agente etiológico da doença. Embora o praziquantel seja o principal medicamento usado para o tratamento, seu uso contínuo levanta preocupações sobre o surgimento de cepas resistentes ao medicamento. A publicação do genoma do *S. mansoni* revelou um grupo de proteínas codificadas por genes Micro-Exon (MEGs), caracterizadas por múltiplas isoformas e exons pequenos e altamente conservados que permitem o splicing alternativo. Dentre estas, a proteína MEG3.3 destaca-se por apresentar expressão aumentada em ovos, enquanto a MEG3.4 apresenta maior expressão na glândula esofágica do *S. mansoni*. Tais padrões de expressão indicam que ambas as proteínas, por estarem presentes na interface parasito-hospedeiro, podem desempenhar papel relevante na modulação dessa interação e representar possíveis alvos terapêuticos. O presente estudo investiga as proteínas MEG3.3 e 3.4 por meio de expressão recombinante, purificação, caracterização biofísica e análise de sua interação com Zn^{2+} e Cu^{2+}. Os resultados revelaram que a MEG3.4 sofre alterações conformacionais em sua estrutura secundária induzidas pela adição de Zn^{2+}. Para a MEG3.3, assim como observado para a MEG3.4, o espectro de dicroísmo circular revelou mudanças conformacionais em sua estrutura secundária induzidas pela titulação de Zn^{2+} e Cu^{2+}. Ensaios de espalhamento dinâmico de luz e crosslinking químico demonstram a formação de oligômeros sob as mesmas condições, confirmando a participação crítica dos grupos tióis como sítios de coordenação para a ligação de Zn^{2+} e Cu^{2+}. De forma análoga às metalotioneínas, a MEG3.3 foi capaz de realizar uma elevada inibição de radicais livres por meio de ensaios de $ABTS^{+}$. Tais descobertas aprofundam a compreensão sobre proteínas codificadas por MEGs, ainda pouco caracterizadas, revelando propriedades estruturais e funcionais até então desconhecidas. Além disso, esses achados podem orientar o desenvolvimento futuro de estratégias terapêuticas voltadas às proteínas MEGs como fatores-chave envolvidos na sobrevivência do *S. mansoni*.

1. INTRODUCTION

1.1. Contextualization of the problem

Schistosomiasis is a neglected tropical disease that impacts over 280 million people in 78 countries, being endemic in 52 of these countries, with 12,858 deaths per year registered in 2021 (Li et al., 2025), primarily in low- and middle-income nations, making it the third most commonly reported tropical disease globally (McManus et al., 2018; Molehin, 2020; “WHO GUIDELINE on control and elimination of human schistosomiasis”, 2022).

The disease is caused by trematode parasites of the genus *Schistosoma*, where the adult worms, both male and female, inhabit the veins of their human hosts. The average lifespan of these worms within their hosts ranges from 3 to 10 years, though confirmed cases have indicated a longevity of up to 37 years (Vieira et al., 2007).

Schistosomiasis in humans is caused by five species of flatworms belonging to the genus *Schistosoma* (*S. mansoni, S. japonicum, S. mekongi, S. guineensis,* and *S. haematobium*). Among these, three are particularly relevant for human infection: *Schistosoma haematobium, Schistosoma mansoni,* and *Schistosoma japonicum*. *S. haematobium* and *S. mansoni* exhibit a broad geographical distribution, occurring in both Africa and Middle East. However, only *S. mansoni* is presented in the Americas. In contrast, *S. japonicum* is predominantly located in Asia, with emphasis on the Philippines and China (Colley et al., 2014; Kokaliaris et al., 2022).

The geographical spread of the disease is limited by the presence of specific species of freshwater snails (Colley et al., 2014). In Brazil, schistosomiasis affects a significant portion of the population, manifesting as endemic in the Northeast and Southeast regions. States registering the highest proportions of positive cases in municipalities with a population of up 500,000 inhabitants were: Sergipe (10.67%), Pernambuco (3.77%), Alagoas (3.35%), Minas Gerais (5.81%), and Bahia (2.91%). Municipalities with over 500,000 inhabitants in Rio de Janeiro (2.80%), Pernambuco (2.48%), and Sergipe (2.28%) also reported positive rates (Katz, 2018).

This high positive rate for this disease is accompanied by a high rate of medication use, specifically by praziquantel drugs. While praziquantel is

highly effective against adult schistosomes, its exclusive use as a monotherapy raises concerns about potential treatment failures due to the possible emergence of drug-resistant parasites. An additional limitation is the lack of significant efficacy against juvenile worm forms (Doenhoff et al., 2002). It is also essential to note that praziquantel does not confer protection against reinfection, a critical point associated with the increase in rates of this disease (Colley et al., 2014; Molehin, 2020).

Some of the main challenges in researching this parasite include the complexity of its life cycle, the intricate structure of the tissues involved, and the limitations of available genetic and transgenic methods for manipulating genes of interest (Li et al., 2018; Naidoo; Mkhize-Kwitshana, 2022; Suttiprapa; Rinaldi; Brindley, 2012; You et al., 2021). Furthermore, this is linked to the complex and critical immune evasion strategies developed by the worms when infecting the human host (Hambrook; Hanington, 2021).

1.2. Immune Evasion Strategies of Schistosomes

Prior to establishing an infection within the definitive human host, *S. mansoni* undergoes a complex development cycle within freshwater snails, which serve as intermediate hosts (**Fig. 1**). This phase involves the transformation of the miracidium stage into cercariae through asexual reproduction. Once maturation is complete, the cercariae emerge from the snail into the aquatic environment to actively seek and penetrate the skin of the definitive host, initiating both tissue invasion and immune evasion strategies (Hambrook; Hanington, 2021).

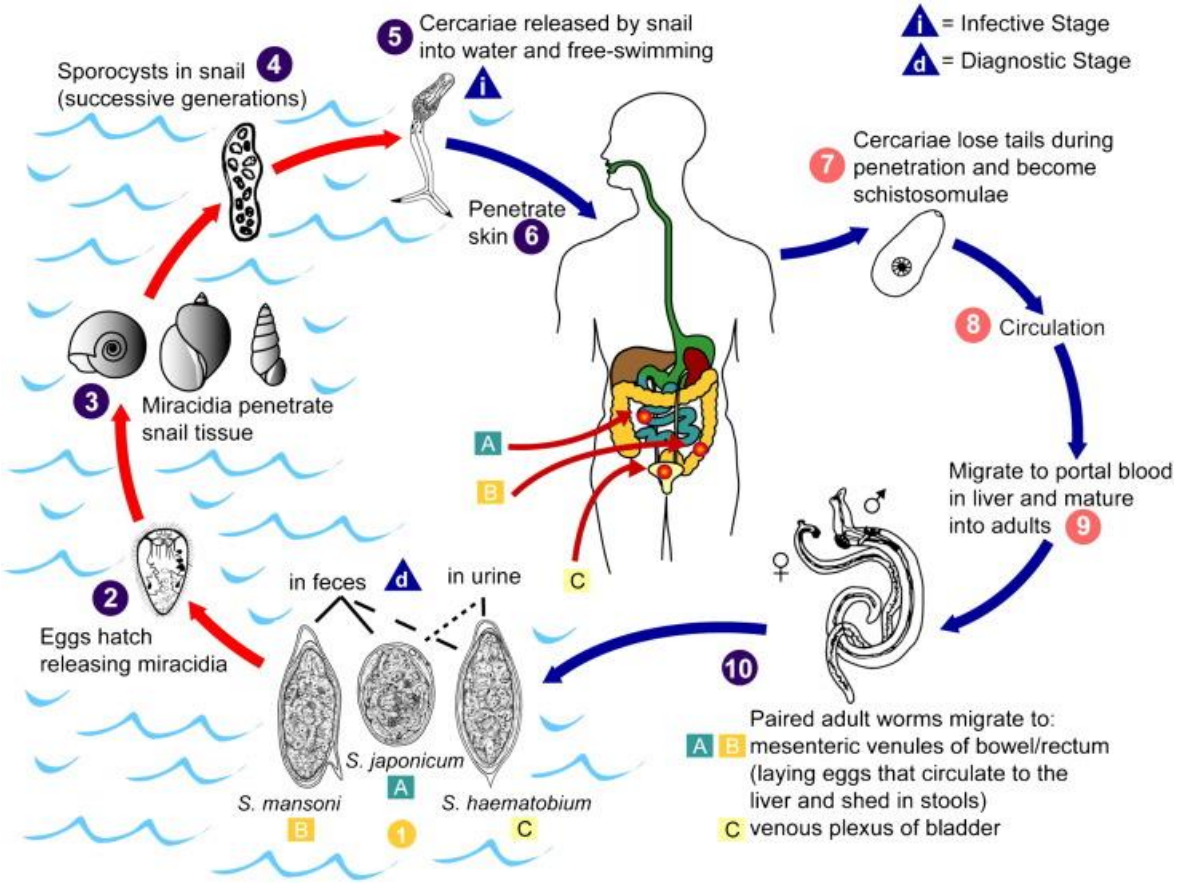

Fig. 1. Schistosome life cycle. The stages of the schistosome life cycle (1–10) include (1) elimination from the host as eggs in feces or urine (diagnostic stage), (2) hatching of miracidia, (3) infection of species-specific aqueous snail intermediate hosts, (4) proliferation of sporocysts within snails, (5) release of cercariae into water (infective stage), (6) infection of host by skin penetration, (7) development into schistosomula, (8) circulation, (9) maturation within portal vasculature, and (10) migration of paired adult worms to target organs. Elimination of schistosome eggs in either feces or urine depends on whether the adults reside in the mesenteric venules of the bowel/rectum (primarily (A) *Schistosoma japonicum* and (B) *Schistosoma mansoni*) or in the venous plexus of the bladder (primarily (C) *Schistosoma haematobium*), respectively (Rose et al., 2014).

1.2.1. Skin penetration

As Hambrook & Hanington (2021) reported, cercariae of *S. mansoni* must penetrate through the epidermis, basement membrane, and dermis in order to locate a venule or lymphatic vessel that will subsequently lead them to the lungs.

Studies suggest that there are several candidates that mediate this anti-inflammatory response at the first contact between cercariae and skin. It was demonstrated that *Sm*16 protein can alter cytokine profiles in mice assays (Curwen et al., 2006). Similarly, homologous proteins from *Schistosoma japonicum* exhibit immunomodulatory properties, including the inhibition of macrophage maturation and the modulation of cytokine production (Hu et al., 2009).

In addition, other less well-characterized immunomodulators also contribute to the infection process. A 23 kDa *S. mansoni* protein has been reported to induce an apoptosis-inducing factor and is associated with immunomodulatory activity through the direct targeting of T cells (Chen et al., 2002).

Although invasive cercariae and cutaneous stage schistosomula secrete a wide variety of factors, the strategy of schistosomes goes beyond the simple release of immunomodulatory molecules to evade the immune response in the skin. Parasite survival requires more than just evasion; it must actively neutralize opsonization by immunoglobulins and complement proteins. Consequently, the organism utilizes a combination of surface-bound factors and excreted molecules to disrupt both innate and adaptive immunity. This transition occurs rapidly; within the first three hours of infection, the schistosomulum sheds its cercarial glycocalyx. Although this carbohydrate-rich layer is vital for osmotic protection in freshwater environments, it becomes a dangerous liability in the host´s skin, where it acts as a primary trigger for the complement system's classical and alternative pathways (Hambrook; Hanington, 2021; Marikovsky et al., 1986).

1.2.2. Lung maturation

Once cercariae successfully penetrates the human host's skin, and reaches a venule or lymphatic vessel, they start the migration to the lungs, where they will mature for a few days prior to continuing to the liver (Hambrook; Hanington, 2021). Some studies indicate that immune mediators employed during skin invasion continue to be utilized during the lung stage (Chai et al., 2006). However, our understanding of the factors secreted by lung-stage schistosomes remains limited, primarily because they are notoriously difficult to isolate.

This knowledge gap is further widened by a historical research bias toward skin-stage larvae as vaccine candidates, along with a significant lack of uniformity in the protocols used for the *in vitro* cultivation and transformation of lung-stage organisms.

In this stage also, schistosomes must be able to withstand the cytotoxic effects of reactive oxygen and nitrogen species in order to survive. Indeed, El Ridi et al. (2010) reported that immune responses generating these reactive species are correlative with larval death. In this context, another study demonstrated that Schistosomes switch from aerobic to anaerobic metabolism during the first two weeks withing the definitive host (Fouad Ahmed et al., 1997), a transition that has been hypothesized to contribute, at least in part to increased resistance to nitric oxide mediated killing (Gobert; Chai; McManus, 2007).

1.2.3. Adult's stage

Adult schistosomes employ a sophistical array of strategies to persist within the hostile environment of the host's mesenteric blood vessels. A primary defensive mechanism is the active incorporation of host-derived antigens, such as major histocompatibility complex (MHC) class I and Fc portion of IgG, onto their heptalaminate tegument (Acharya; Da'dara; Skelly, 2021; Torpier; Capron; Ouaissi, 1979). By binding host proteins in specific orientations, the parasite masks itself from detection and renders antibodies unable to signal to effector cells like macrophages and eosinophils, effectively blocking antibody-dependent cellular cytotoxicity (Hambrook; Hanington, 2021). Additionally, adult worms utilize molecular mimicry by producing neuropeptides like adrenocorticotropic hormone, which inactivates host leukocytes and blunts the Th1 immune response (Salzet; Capron; Stefano, 2000).

To survive long-term within the vasculature, adult schistosomes also release specific excreted products to manipulate the surrounding physiological and immunological milieu. These include potent serine protease inhibitors, such as SmKI-1, which protect the parasite from neutrophil elastase-mediated damage (Morais et al., 2018). Furthermore, the worms have evolved a complex suite of anticoagulants-including SmATPDase1 and various calpains to prevent blood clot formation and platelet deposition (Da'dara et al., 2014; Leontovyč et al., 2018), ensuring their continued mobility and survival within the host´s bloodstream.

1.2.4. Egg's stage

The pathology associated with schistosomiasis is primarily driven by the eggs, which must navigate through host tissues to be excreted (Cheever et al., 1994). To facilitate this migration, the egg through its cell-derived sub-shell envelope-secretes a variety of immunomodulatory factors that harness the host´s immune response rather than merely evading it. Central to this process is the induction of the Th2 type granulomatous response (Pearce, 2005), which is essential for the successful movement of the egg through the intestinal or bladder wall. This skewing of the immune environment is achieved by specialized glycoproteins such as □-1, also known as Interleukin-4-inducing principle of *S. mansoni* eggs (IPSE), which triggers IL-4 production in basophils and promotes the development of regulatory B cells to manage local inflammation (Schramm et al., 2007).

In addition, the egg release ω-1 , a T2 ribonuclease that serves as a primary driver of the Th2 response by targeting dendritic cells (Everts et al., 2009). Once internalized via mannose receptors ω-1 degrades host mRNA and rRNA, effectively suppressing protein synthesis and altering antigen presentation. Beyond these main glycoproteins, the egg stage utilizes *Sm*CKBP to reduce the recruitment of inflammatory leukocytes by binding host chemokines like CXCL8 and CCL3 (Smith et al., 2005). To ensure survival against cellular attacks, the egg also produces the Kunitz-type serine protease inhibitor SmKI-1 to block neutrophil elastase, while factors like *Sm*Enolase and *Sm*Calp1 are thorough to facilitate the physical degradation of host fibrin and connective tissue during the exit process (Figueiredo et al., 2015; Wang; Da'dara; Skelly, 2017).

1.3. Micro-Exon Genes (MEGs)

The publication of the *S. mansoni* genome revealed the presence of distinct genes called micro-exon genes (MEGs) (Berriman et al., 2009). The most recently annotated version of the *S. mansoni* genome features at least 35 unique MEG genes (Nedvědová et al., 2023). These genes have a peculiar structure, composed of 10 to 20 very short exons alternated with long introns. The short exons are, in most cases, multiples of three, ranging from a

minimum of 6 base pair (bp) (encoding two amino acids) to a maximum of 81 bp. The majority of exons are 15 bp long, thereby encoding five amino acids (Berriman et al., 2009; Howe et al., 2017; Nedvědová et al., 2023).

This gene configuration, which is composed of small exons (**Fig. 2**), enables the removal of one of the exons from the mature transcript through alternative splicing, without causing a disruption in the transcript's reading frame (Berriman et al., 2009). In *S. mansoni*, studies show that 35 MEGs are encoding at least 87 verified MEG proteins, most of them originating mainly from alternative splicing of the central exons (Nedvědová et al., 2023).

The MEG families encoded unrelated proteins with unknown functions and do not exhibit conserved domains. Orthologues of *S. mansoni* MEGs have been exclusively identified in other organisms belonging to the genus *Schistosoma* and in *Trichobilharzia regent* (Li et al., 2018). The presence of a signal peptide is a characteristic shared by most MEGs, suggesting they are secreted proteins. They have been previously detected in the secretions of eggs, schistosomula, and adult worms (DeMarco et al., 2010)

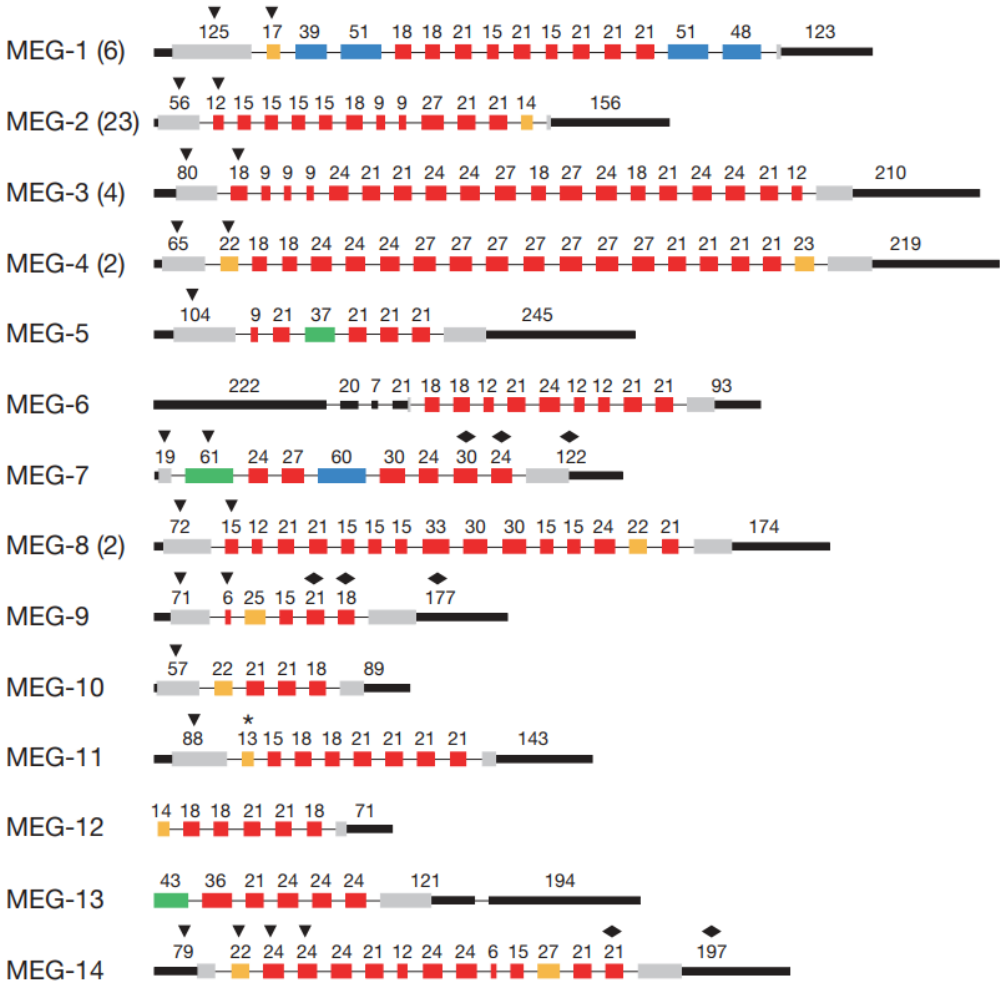

Fig. 2. Schematic representation of MEGs in *Schistosoma mansoni*. Numbers in parenthesis indicate the multiple MEG variants belonging to that family. Rectangles denote exons, and thin lines represent introns. Thick lines at the ends indicate untranslated regions (UTR) regions. Red rectangles are symmetric micro-exons (<36 bp), orange are asymmetric micro-exons. Blue rectangles are normal symmetric exons, and green are normal asymmetric exons. Grey rectangles represent the coding region of adjacent exons. Exons with triangles above code for a signal peptide, and those with a diamond code for transmembrane regions (Berriman et al., 2009).

1.3.1. MEG 3.3 and MEG3.4

Research indicates that MEG family undergoes significant regulation through the life cycle of *S. mansoni*, with a distinct preference for expression during the intramammalian phases (Berriman et al., 2009; DeMarco et al., 2010) and, these proteins are recognized as major constituents of the egg's secretome. Bioinformatic analysis initially predicted the secretion of MEG3 families based on the identification of the signal peptide sequences (DeMarco et al., 2010). These predictions were later validated through proteomic analysis of *S. mansoni* eggs, which also confirmed the existence of multiple isoforms as results from extensive alternative splicing.

Sequence analysis yielded limited information regarding the biological functions of these proteins, that is why we require their local expression, therefore provides critical functional clues. In adult parasites, MEGs are found within the esophageal gland, where MEG3.4 is highly expressed in the section near to the worm's head (Wilson et al., 2015) (**Fig. 3**), suggesting that they may interact with host leukocytes during blood feeding, acting likely facilitating tissue passage or immune evasion through direct interaction with host molecules.

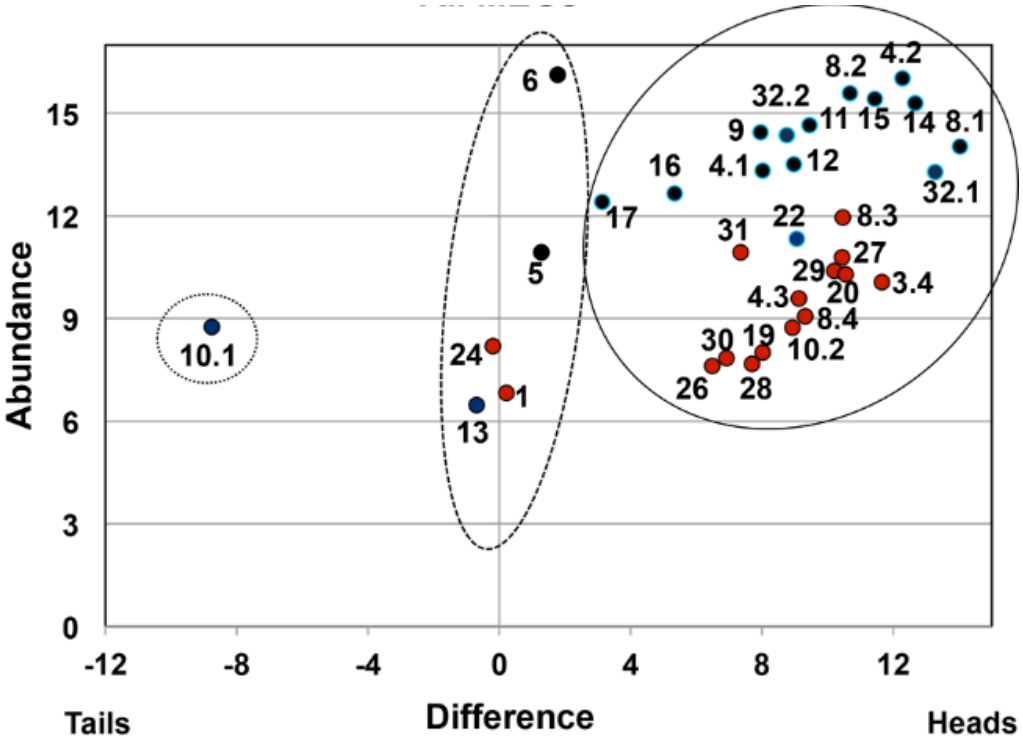

Fig. 3. Scatter plot of all MEGs identified in the esophagus study. The MEGs found by Cufflinks mapping (black circle) are distinguished from those located only by Trinity de novo assembly (red circle), and MEG families found to be highly enriched in the head preparation, including those previously known (blue labels/circles). The MEGs fail into three distinct populations: (i) solid line, fourfold in the heads>tails; (ii) dashed line, heads=tails; (iii) dotted line, tails>heads (Wilson et al., 2015).

However, in the context of the egg stage, MEG3 proteins (specifically isoforms such as MEG3.3) emerge as priority targets for study due to their abundance in the egg secretome and their presence in the sub-shell envelope. Together with MEG2 (Berriman et al., 2009), MEG3 contributes to the structural organization of the egg sub-shell and has also been implicated in the migratory behavior of schistosomula (Štěpánka Nedvědová, 2023). This association is supported by the higher

expression of these genes in mature eggs compared with immature eggs (**Fig. 4**).

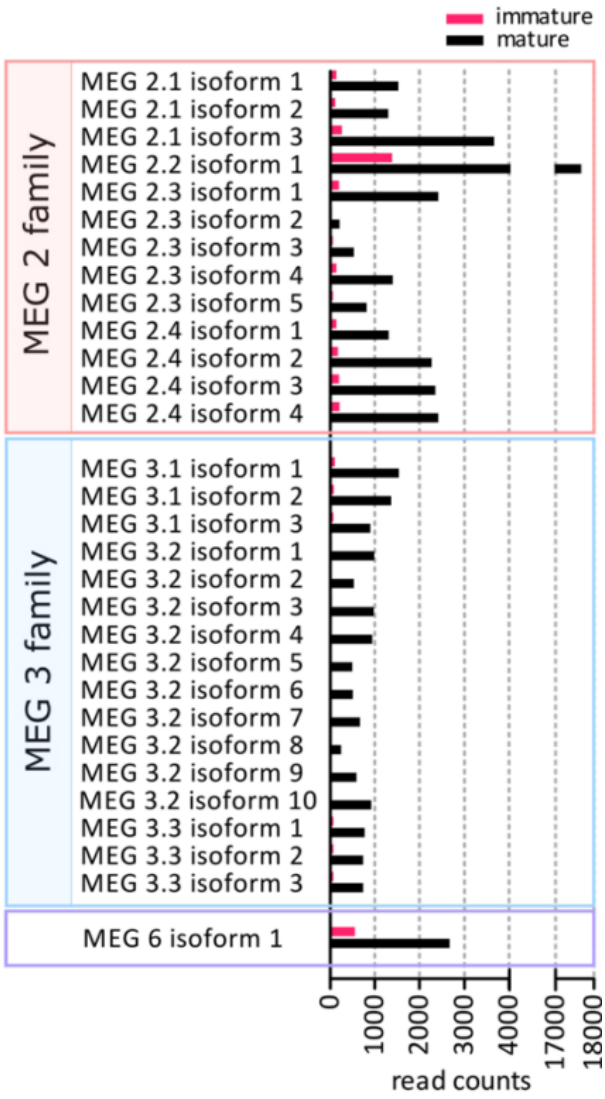

Fig. 4. Comparison of MEG Protein Expression in Mature and Immature *Schistosoma mansoni* Eggs. Expression levels were quantified using illumina platform short reads obtained from RNA isolated from *S. mansoni* eggs. Preliminary, unpublished data from the Dvorak laboratory (2023) indicates significantly higher expression of MEG proteins in mature eggs compared to immature ones. This suggests these proteins play an essential role during maturation and in the potential interaction with host tissues. The analysis highlights the importance of MEG proteins at specific stages of egg development (Štěpánka Nedvědová, 2023).

Additionally, the focus on MEG3 family proteins is due to their small size, ranging from 13 to 16 kDa, and the singular characteristics of its eight conserved cysteine pairs with a C3XC motif, an unusually high number of cysteine residues for small proteins. The biological versatility of the MEG family is further evidenced by its diverse localization across

various life cycle stages. It is proposed that MEG proteins secreted by both larvae and egg function to interact with and modify the host´s vascular endothelium. Such differential distribution suggests that while these MEG share a unique genetic origin, their various isoforms have evolved to perform distinct and vital roles in the survival and pathogenesis of *S. mansoni*.

1.4. Metallothionein proteins

The metallothionein proteins are low molecular weight proteins that have shown interesting activity in homeostasis by binding some ions like Zn^{2+}, Cu^{2+}, Cd^{2+} and Hg^{2+}, via thiol groups in their cysteine-rich sequences (Atrian; Capdevila, 2013; Penkowa; Hidalgo, 2001), a similar characteristic shared with MEG3 CX3C motif. Zn^{2+} and Cu^{2+} ions are crucial for healthy immune system, specifically supporting immune cell development, functions of macrophages and T cells, and fighting infection by creating toxic environments for pathogens (Hambrook; Hanington, 2021). In fact, studies indicate that extracellular metallothionein plays a role in controlling T cell proliferation, inflammation, and apoptotic processes (Howe et al., 2017; Lu; Woodburn, 2005).

These specific hypothesized activities are attributed to their distinctive structural features, particularly the presence of eight conserved cysteine pairs arranged in a CX3C motif. Studies have shown that CX3C can bind to zinc ions, as seen in the protein Tim10 (Lu; Woodburn, 2005). Additionally, theCX3C motif of fractalkine is recognized by the specific receptor CX3CR1**,** which is expressed on immune cell membranes, including T cells and monocytes (Liu et al., 2019). These observations suggest that CX3C-containing motifs may participate in interactions with immune-cell receptors, an important component of immune homeostasis (Sutherland; Stillman, 2011).

Collectively, these findings support the hypothesis that recombinant MEG3 protein isoforms are able to bind zinc, a metal ion known to play a critical role in modulating the human response.

1.5. Justification of the study

The esophageal gland, an accessory digestive organ, plays a crucial role in the survival of *Schistosoma mansoni* within the mammalian host. It has been directly associated with immune evasion mechanism, helping the parasite escape immune system defense (Lee; Chong; Newmark, 2020).

Similarly, higher expression in eggs is associated with increased biological activity and an important role in parasite survival. The elevated expression of MEGs in both the esophageal gland and eggs suggests that these proteins may play a significant role in modulating the human immune response (Wilson et al., 2015).

Biochemical and structural characterizations of MEG proteins may provide important insights into their functions and interactions with the host immune system, as illustrated by MEG14, which interacts with the human pro-inflammatory protein S100A9 (Orcia et al., 2017).

The study of MEG3 family is of great interest, as the worm's esophageal gland and eggs participates as part of *Schistosoma mansoni*'s immune evasion strategies (Hambrook; Hanington, 2021).

2. OBJECTIVES

2.1. General objective

The present project aims to investigate MEG3.3 and MEG3.4, which are predominantly expressed in the eggs and esophagus from *Schistosoma mansoni* adult worms, respectively, through recombinant expression and biophysical characterization using techniques such as circular dichroism, dynamic light scattering, chemical crosslinking, and antioxidant capability.

2.2. Specific objectives

Express and purify MEG3.3 and MEG3.4 recombinant proteins in *E. coli*.

Evaluate and compare the structural architecture of MEG3.3 and MEG3.4 using *in silico* modeling.

Characterize the secondary structure and metal-induced conformational changes of the recombinant proteins.

To evaluate whether the proteins display scavenging activity and to examine the possible effects of metal coordination on this potential antioxidant activity.

3. METHODOLOGY

3.1. Sequences Analysis

The amino acid sequences of MEG3.3 and MEG3.4 were retrieved from the National Center for Biotechnology Information (NCBI) database. Signal peptides were identified using the *SignalP* 5.0 (Almagro Armenteros et al., 2019). Subsequently, the mature sequences (excluding the signal peptides) were analyzed using the *ProtParam* tool on the *ExPASy* server (Gasteiger et al., 2005) to determine their physicochemical properties. Sequence alignment and comparative analysis were performed using Jalview software (Waterhouse et al., 2009).

3.2. Bacterial Strains and Preparation of Competent Cells

The study was performed using different *E. coli* strains, DH5α for plasmid propagation, BL21 (DE3) and Rosetta-Gami2 (DE3) pLysS (Novagen) for protein expression. All strains were transformed into chemically competent cells. A single colony was inoculated into 2 mL of LB medium and incubated overnight at 37 °C and 150 rpm. This starter culture was then used to inoculate 100 mL of LB medium (0.5 g/L NaCl, 10 g/L tryptone and 5 g/L yeast extract), which was grown at 37 °C until reaching an OD_{600} of 0.5-0.7. The culture was chilled on ice for 10 min, and all subsequent steps were performed at 4 °C. Cells were harvested by centrifugation (5,000 xg for10 min at 4 °C) and gently resuspended in 20 mL of ice-cold 0.1 M $MgCl_2$ and incubated on ice for 30 min. Following a final centrifugation, cells were resuspended in 10 mL of ice-cold 0.1M $CaCl_2$ supplemented with 15% (v/v) glycerol. Aliquots of 200 µL were flash-frozen in liquid nitrogen and stored at -70 °C. Competency was verified via transformation with a control plasmid,

using water as a negative control, and plating on selective and non-selective LB agar.

3.3. Expression and purification of MEGs

3.3.1. Recombinant expression

The coding sequences of MEG3.3 and MEG3.4 were commercially synthesized (FastBio Ltda) and provided already cloned into the bacterial expression vector pET28a+, inserted at the NdeI-BamHI restriction sites.

Plasmid constructs were transformed into *E. coli* DH5α via heat shock for clonal propagation. To evaluate protein expression, the plasmid was subsequently transformed into *E. coli* BL21 (DE3). Initial expression trials resulted in the localization of the target proteins within inclusion bodies. To promote soluble expression and facilitate the formation of the disulfide bonds mediated by the eight cysteine pairs present in the MEG sequences, further transformations were conducted using the *E. coli* Rosetta-Gami2 (DE3) pLysS strains. Small-scale expression tests (20 mL LB medium) were performed and monitored via 15% SDS-PAGE under reducing conditions (with β-mercaptoethanol). Protein bands were visualized and compared against a high-range molecular weight marker (S2600 TrueColor, Sinapse). Upon confirmation of expression, large-scale production was carried out in 1 L of LB medium at 37 °C until reaching an OD_{600} of 0.6-0.8, induced with 0.5 mM isopropyl β-D-thiogalactopyranoside (IPTG) overnight at 18 °C and 150 rpm.

After the expression period, the cell suspension was centrifuged (2,500 xg for 30 min at 4°C), the cells were resuspended in buffer 1 (25 mM HEPES pH 8.0, 150 mM NaCl) or buffer 2 (25 mM Tris-HCl pH 8.0 buffer, 150 mM NaCl) depending the experiment to be performed (HEPES for chemical crosslinking assay only). The cells were lysed (30 s On, 59 s Off, Amplitude 25% for 15 min) using an ultrasonicator VCX500 (Sonics Vibra-Cell) under ice-cold conditions, and the soluble fraction was separated by centrifugation (7,800 xg for 30 min at 4°C). Samples from the pellet and supernatant were taken to assess whether the protein was soluble or insoluble. The inclusion bodies were resuspended in buffer 2, adding 6 M guanidine (Sigma-Aldrich) and 10% of glycerol and then lysed

again by sonication under the same conditions. The sample was then centrifuged again, and the resulting supernatant was subjected to following purifications steps.

3.3.2. Affinity chromatography purification

The supernatant, corresponding to the soluble fraction of the inclusion bodies lysis, was subjected to affinity chromatography using 2 mL of Ni-NTA resin (Qiagen). The resin was washed with buffer 2 including 6M urea, and the protein of interest was eluted with buffer 2 with 6M urea and supplemented with 0.5 M imidazole (each elution were performed with 5 mL).

During the elution process, the protein was monitored by NanoDrop One Microvolume UV/Vis spectrophotometer (Thermo Fisher Scientific) at 280 nm and collected until the absorbance value was less than 0.2 (minimum absorbance of the sample to be visible in SDS-PAGE). Finally, protein samples from the wash and elution fractions were analyzed by 15% SDS-PAGE in reduced conditions (with β-mercaptoethanol) to assess the presence and purity of the target proteins (MEG3.3 and MEG3.4, respectively).

3.3.3. Protein refolding process

Dialysis refolding

Protein collected from the affinity chromatography purification step was subjected to a refolding process using dialysis, because protein was in buffer 2 supplemented with 6M urea and 0.5 M imidazole. The denatured protein (initial concentration 6 M urea) was diluted until reached 0.1 abs (280 nm). In the first attempt, the diluted protein solution was transferred to a 10 kDa molecular weight cutoff (MWC) dialysis membrane (INDICAR MARCA) and dialyzed from 6 M to 0 M of urea against 2 L of buffer 2 overnight, with dialysis performed at either 18 °C or 25 °C.

The second refolding attempt was achieved using a stepwise gradient of dialysis solutions, changing the concentration of urea in the buffer by 2 M decrements until 0 M urea was reached (Sørensen;

Sperling-Petersen; Mortensen, 2003). Different dialysis durations (4, 6, 8 h and overnight) and temperatures (25 and 18 °C) were evaluated.

Finally, the second dialysis condition was performed by adding 0.2 M arginine, and a redox pair of 5 mM cysteine and 0.5 mM cystine in the dialysis solution (Oyeleye et al., 2020), to suppress partial protein aggregation. Insoluble protein was removed by centrifugation (5,000 xg for 30 min at 4 °C), and the recovered protein was concentrated using an Amicon Ultra-15 centrifugal filter with a 10 kDa cutoff (5000 xg for 40 min at 4°C).

Every attempt was monitored comparing the protein absorbance at 280 nm inside the MWC membrane, before and after dialysis process, and by the presence of protein aggregation.

On-Column refolding

An alternative refolding approach was also tested, in which protein refolding was performed while the protein remained immobilized on Ni-NTA resin. In this protocol, the resin was initially washed twice and then subjected to on-column refolding using 5 different series of refolding buffers (each buffer consists in 20 mL) with decreasing urea concentration (6-0 M; 25 mM Tris-HCl pH 8.0, 150 mM NaCl; 0.2 M arginine; 5 mM Cysteine; 0.5 mM cystine; 10% glycerol), progressively reducing the denaturing conditions from 6 M to 0 M urea for each 2 h. The elution buffer (final refolding buffer) was supplemented with 0.5 M imidazole. Finally, samples from the wash and elution steps were analyzed by 15% SDS-PAGE in reduced conditions (with β-Mercaptoethanol) to assess the presence of the protein throughout the on-column refolding procedure (Li; Huang, 2007).

3.3.4. Size Exclusion Chromatography purification

Subsequently, molecular size exclusion chromatography (SEC) was performed using a Superdex 75 column (HR 10/300, Cytiva) coupled to

an AKTA pure system (Cytiva). Aliquots of 1 mL were applied to this system, and aliquots of 1 mL were also collected. Buffer 2 was used to perform SEC, within a flow rate of 0.5 mL/min, and the elution of fractions of interest was monitored by absorbance at 280 nm. Aliquots were taken at each stage of the process for evaluation by 15 % SDS-PAGE in reduced conditions (with β-mercaptoethanol). Purification conditions such as buffer composition and washing were optimized for each protein, that is why we supplemented buffer 2 with arginine, cysteine and cystine.

Elutions from SEC purification were collected and concentrated using an Amicon Ultra-15 centrifugal filter, obtaining MEG3.3 protein at 20 µM of concentration, while MEG3.4 protein was concentrated until 5 µM (before begin to aggregate).

3.4. Secondary structure determination

3.4.1. Structural prediction by AlphaFold

For structural prediction, the signal peptide of each protein were predicted by *SignalP* 5.0, and removed from the sequence, after that, each sequence was submitted to the AlphaFold3 server (Abramson et al., 2024), determining the 3D structure and the degree of confidence predicted.

3.4.2. Circular Dichroism

The recombinant proteins obtained were initially analyzed by circular dichroism (CD) to verify their folding in terms of secondary structure and stability (Kelly; Jess; Price, 2005). The CD spectra were obtained using a Jasco J-815 spectropolarimeter in the wavelength range 200-260 nm, using a 0.1 cm optical path cuvette. The spectra were determined as an average of eight scans at a speed of 50 $nm.min^{-1}$.

Using this technique we also evaluated possible spectral changes associated with interactions with the Zn^{2+} and Cu^{2+}. Spectra were obtained for the proteins alone and after the addition of increasing concentrations of Zn^{2+} and Cu^{2+} until proteins precipitation was observed, in order to assess potential conformational changes in secondary structure. For the assays, MEG3.3 was used at 20 µM and MEG3.4 at 5

μM (maximum protein concentration obtained, respectively), both in 25mM Tris-HCl pH 8.0 and 150 mM NaCl.

All measurements obtained were normalized, converting the units to Δε using the *CDtoolX* software (Miles; Wallace, 2018).

3.5. Zinc and copper binding capability

3.5.1. Structural binding prediction

For structural and binding prediction, the protein sequence without the signal peptide was submitted to the AlphaFold3 server (Abramson et al., 2024). To investigate the 3D structure of protein-ion interaction, we simulate the interaction between each MEG protein in the presence of increasing numbers of the corresponding ions. The model exhibiting the highest confidence scores across independent predictions was selected as the most reliable representation of the protein-ion interaction.

3.5.2. Chemical Crosslinking

For chemical crosslinking assays using disuccinimidyl suberate (DSS), HEPES buffer was chosen because it lacks primary amines and is therefore chemically inert towards NHS esters. The use of Tris-HCl based buffers were avoided, as their primary amines compete with the lysine residues of MEG proteins, acting as quenching agents and reducing the efficiency of the intermolecular adduct formation reaction.

Ligand-induced changes in protein oligomeric state were assessed by incubating the purified protein at a concentration of 20 μM with three ligands concentrations (50 μM, 100 μM, and 500 μM) for 30 minutes at room temperature.

Next, 1 mM of DSS was added and incubated for 1 h at 25 °C. All samples were analyzed by 15 % SDS-PAGE to observe changes in protein molecular weight due to oligomerization, comparing the bands to the protein in its apo form.

Additionally, to evaluate whether specific oligomeric changes were specifically mediated by thiol groups from cysteine residues, samples were pre-treated with 1 μM of dithiothreitol (DTT) to reduce disulfide bonds prior to ligand incubation and the DSS crosslinking reaction.

Samples were then analyzed by 15 % SDS-PAGE in reduced conditions (with β-mercaptoethanol) to assess alterations in the bands in comparison to the chemical crosslinking performed first.

3.5.3. Particle size by Dynamic Light Scattering

Dynamic light scattering (DLS) experiments were conducted using a Litesizer 500 (Anton Paar GmbH, Graz, Austria) to determine the particle size of the protein incubated with ligands. The instrument employs a 3 mW laser with a wavelength of λ = 658 nm and performs measurements at a backscattering angle. All samples were analyzed in ultramicro quartz cuvettes with a 10 mm path length (Hellma Analytics, Müllheim, Germany) at a controlled temperature of 25 °C (Skrzyniarz et al., 2024). For these experiments study, MEG3.3 at 20 µM was incubated with increasing concentrations of each ion (10, 50, 100, 200 and 500 µM).

3.6. Antioxidant capability

The radical scavenging properties were evaluated by antioxidant activity using 2.2'-azino-bis (3-ethylbenzothiazoline-6-sulfonic acid) (ABTS) method (Re et al., 1999) with some modifications. ABTS reagent was prepared in the water to obtain a 10 mmol L^{-1} stock solution. The ABTS radical cation ($ABTS^{+}$) was produced by reacting 1.0 mL of the ABTS stock solutions with 430 µL of potassium persulphate (8.17 mM). The mixture was shaken and kept in the dark at room temperature for 16 h, this solution was diluted and adjusted to 0.511 mM.

Subsequently, in 96-well plates, 25 µL of the $ABTS^{+}$ solution was added to 100 µL of the sample (protein of interest at concentration of 20 µM in 25 mM Tris-HCl pH 8.0, 150 mM NaCl and 10 % glycerol.

The absorbance at 755 nm (abs_{755}) was recorded at 5 min intervals, for 60 min, using a microplate spectrophotometer (Biotek Synergy H1). The microplate was automatically shaken before each reading. The $ABTS^{+}$ solution without the test compounds was used as a control, and the percentage of $ABTS^{+}$ scavenging was calculated with equation (1).

$$\%ABTS^{+} = \frac{abs_{755}(control) - abs_{755}(sample)}{abs_{755}(control)} \times 100 \quad (1)$$

Therefore, the radical scavenging activity was expressed as the percentage reduction in ABTS+ absorbance relative to the negative control (ABTS+ solution without protein).

4. RESULTS

4.1. Initial Analysis of protein sequences

The MEG3.3 protein comprises 151 amino acids residues, of which 20 correspond to the predicted signal peptide and 131 to the helical domain (**Fig. 5**). Similarly, MEG3.4 protein contains 156 amino acids residues, including 18 from the signal peptide and 138 from the helical domain, also shown in **Fig. 5**. The signal peptides were predicted using the *SignalP* tool.

The sequence analysis allows the identification of specific amino acids residues useful for monitoring purification, such as tryptophan (Trp), an aromatic residue with strong absorbance at 280 nm. Notably, MEG3.4 contains Trp in its sequence, whereas MEG3.3 lacks Trp but contains four phenylalanine residues (Phe), also an aromatic amino acid residue that absorb at 257 nm.

Sequence alignment of MEG3.3 and MEG3.4 also revealed a total of 16 cysteine (Cys) residues in each protein. This unusually high cysteine content for proteins of this size is relevant for expression and purification strategies and may be functionally significant, although the biological roles of these proteins remain to be elucidated.

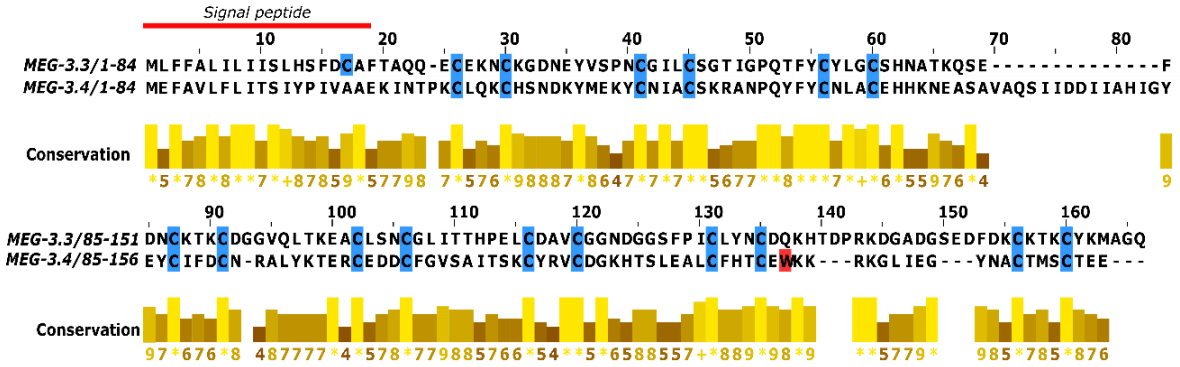

Fig. 5. Primary sequences alignment of MEG3.3 and MEG3.4 proteins. The red line indicates the predicted signal peptide at the N-terminus. Key residues are highlighted by color: blue (cysteine), and red (tryptophan). The conservation track and yellow histogram bars represent the evolutionary similarity and consensus between the two sequences at each amino acid position, with a 25.77 % of identity.

Similarity, the theoretical physicochemical properties of MEG3.3 and MEG3.4 proteins (without signal peptides), such as molecular mass and theoretical isoelectric point (pI), which were obtained by submitting the primary structures to the *ProtParam* tool available on the *Expasy* server (Table 1).

Table 1. Theorical parameters of the MEG3.3 and MEG3.4 proteins.

Protein	Molecular weight (Da)	Number of amino acids residues	Theoretical pI	Ext. Coefficient ($M^{-1}cm^{-1}$)	Abs_{280nm} 0.1% (1g/L)
MEG3.3	14118.72	131	5.07	7450	0.528
MEG3.4	15870.07	138	6.65	18910	1.192

4.2. Expression and Purification

Heterologous expression of MEG3.3 and MEG3.4 were performed in *E. coli* BL21 (DE3) cells following transformation with the corresponding expression constructs. To evaluate protein expression and solubility, isolated colonies were selected and grown at 37 °C until reaching an OD_{600} of 0.6-0.8, after which protein expression was induced with 0.5 mM IPTG, and culture were incubated overnight at 18 °C.

Proteins expressions were analysed by 15% SDS-PAGE in reduced conditions (with β-mercaptoethanol) using aliquots collected before and after induction. MEG3.3 and MEG3.4 was successfully expressed in the BL21 (DE3) cells (**Fig. 6**), showing an apparent molecular mass of approximately 15 kDa, consistent with the predicted molecular masses derived from the amino acid sequences, 14.1 kDa for MEG3.3 and 15.8 kDa for MEG3.4, as shown in **Fig. 6**, lanes of induced MEG3.3 and M3G3.4 samples, respectively.

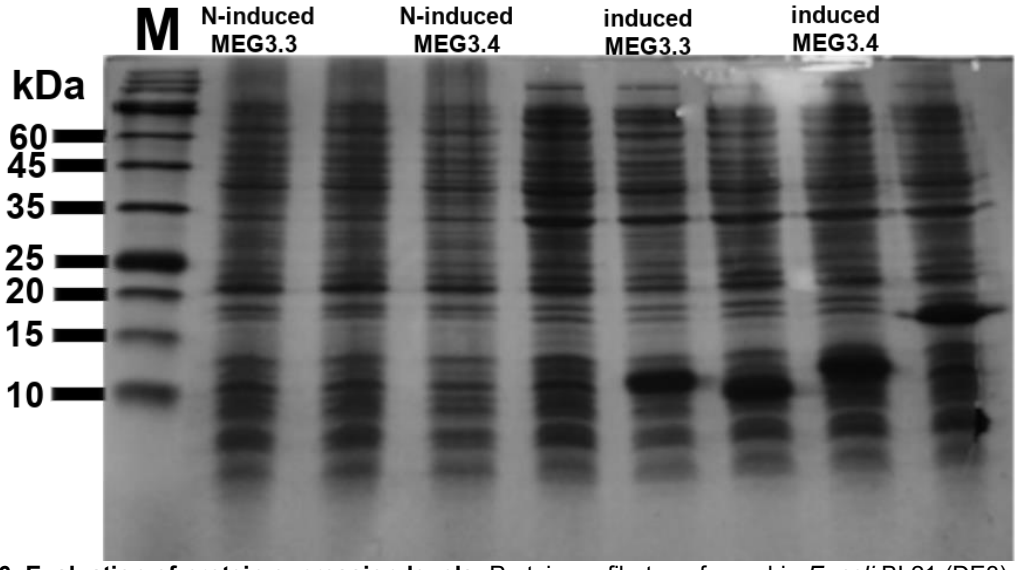

Fig. 6. Evaluation of protein expression levels. Protein profile transformed in *E. coli* BL21 (DE3) with the pET-system. The protein molecular weight marker is in kDa (**M**), and non-induced **(N- induced)** samples of MEG 3.3, and 3.4, and other proteins, as well as induced samples. The increased band intensity in induced lanes confirms successful recombinant over-expression.

After the expression test, aliquots from the same colonies were collected and stored at -70 °C, meanwhile all samples expressed were used to perform the solubility and purification test.

The solubility test for MEG3.3 is illustrated in **Fig. 7-A**. SDS-PAGE analysis revealed a prominent band in the insoluble fraction indicating that MEG3.3 is predominantly localized in inclusion bodies. This observation supported the use if affinity chromatography under denaturation conditions, which resulted in a strong band corresponding to denatured MEG3.3 in the final elution fraction. Similarly, the solubility test for MEG3.4 (**Fig. 7-B)** also indicated accumulation in inclusion bodies.

All samples analysed by 15 % SDS-PAGE in reduced conditions (with β-mercaptoethanol) were derived from affinity purification of the insoluble fraction and showed a denatured protein band that was more intense than that observed for MEG3.3. Notably, the band was already visible in the wash fractions and increased in intensity toward the final elution, suggesting partial protein loss during washing steps and confirming higher expression levels of MEG3.4 compared to MEG3.3.

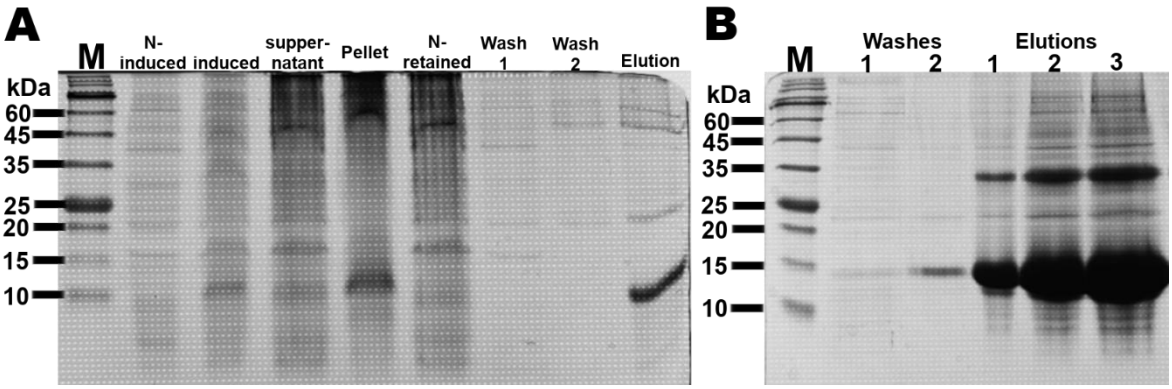

Fig. 7. Purification of MEG3.3 and MEG3.4 by Nickel Column Affinity in SDS-PAGE. (**A**) Protein profile of MEG3.3 purification, lanes correspond to protein molecular weight marker (**M**), non-induced (**N- induced**), and samples from each step of purification. (**B**) Protein profile of MEG3.4 purification, showing the last washes and respective elutions with a high protein concentration.

The refolding process was performed by dialysis, with decreasing urea concentrations (6-0 M) in 2 L of the same protein purification buffer at 25 °C overnight. Protein absorbance at 280 nm was measured before and after dialysis to monitor recovery. For MEG3.3 no visible precipitation was observed, and the absorbance did not show significant variations, indicating successful refolding and yielding a protein suitable for subsequent purification process.

However, for MEG3.4, the first dialysis protocol resulted in protein precipitation, as shown in **Fig. 8**. Therefore, several variations of the dialysis procedure were tested exclusively for MEG3.4 in an attempt to obtain properly refolded protein for subsequent assays. These modifications included a gradual reduction of 2 M urea, from 6M to 0 M in order to achieve a smoother transition from denaturing to native conditions. Additionally, buffer exchange intervals of 4, 6, and 8 hours, as well as overnight, were evaluated, and refolding was tested at both 25 °C

and 18 °C. Despite these adjustments, MEG3.4 consistently tended to precipitate under all conditions tested.

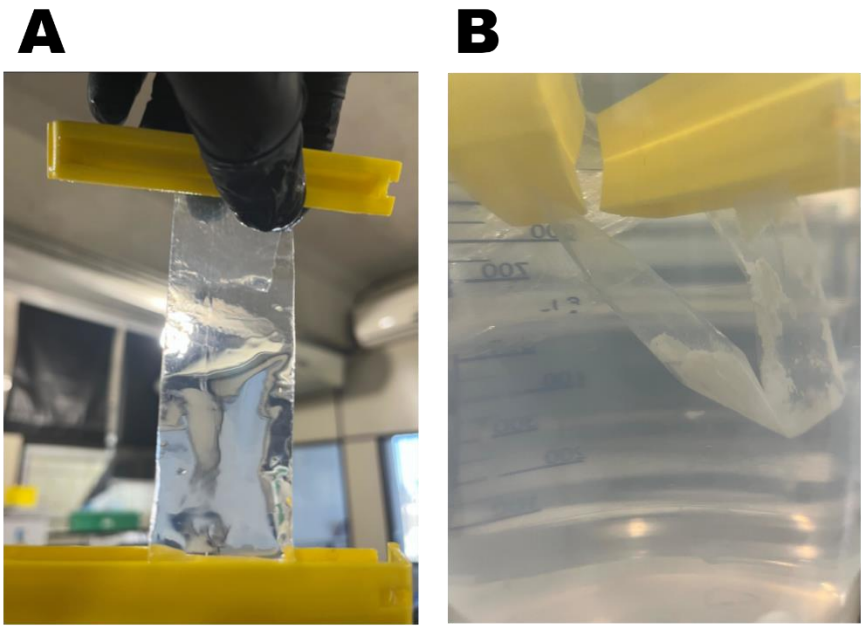

Fig. 8. Dialysis of MEG3.4. (A) MEG3.4 protein eluted from affinity chromatography at the beginning of the refolding process. (**B**) The protein precipitated after dialysis.

In the final refolding attempts, the inclusion of 0.2 M arginine partially reduced protein aggregation, and no visible precipitation was observed as previously seen in **Fig. 8-B**.

Following affinity chromatography purification and refolding process, MEG3.3 and MEG3.4 were subjected to Size Exclusion Chromatography (SEC), as both proteins were close to 15 kDa in molecular weight, this purification was performed using a Superdex75 10/300 GL column with an isocratic flow of 25 mM Tris-HCl pH 8.0, 150 mM NaCl and 10% glycerol, depending on the experiment.

The SEC purification of MEG3.3 was successful, showing a single, symmetric peak at fraction collected at 15 mL in **Fig. 9-A**, migrating below the 15 kDa molecular weight marker and consistent with the predicted molecular mass of 14.1 kDa. This procedure yielded MEG3.3 at approximately 15 µM, which was subsequently concentrated to 20 µM using an Amicon Ultra-15 centrifugal filter.

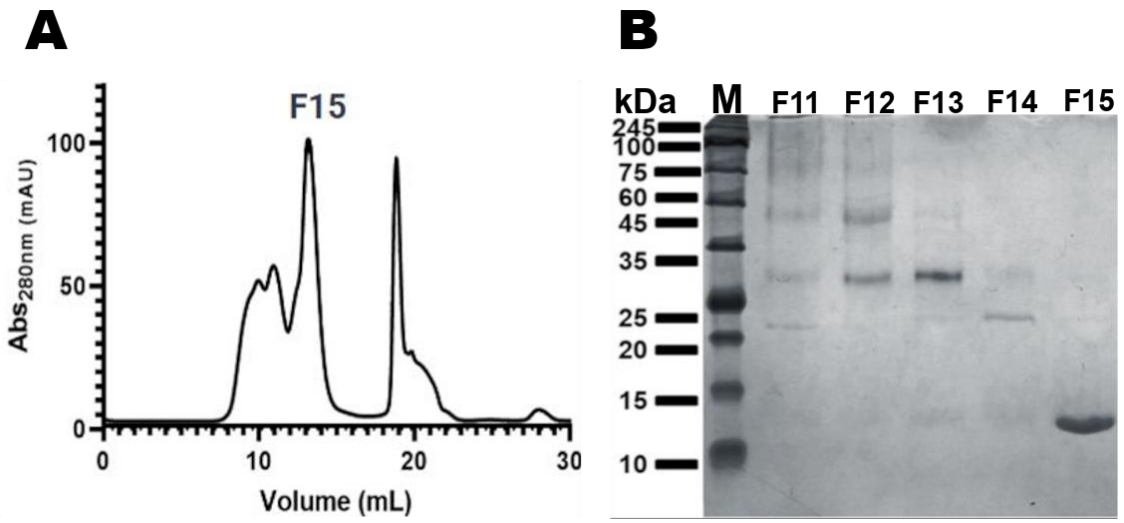

Fig. 9. Size Exclusion Chromatography and SDS-PAGE analysis of MEG3.3 fractions. (**A**) Protein profile of MEG3.3 purification by SEC using a Superdex75 Increase 10/300 GL column with an isocratic flow showing the fraction collected at 15 mL (**F15**) of interest; fractions/elution volume were collected and analyzed by (**B**) SDS-PAGE, showing the protein molecular weight marker in kDa (**M**) and the following fractions: fraction collected at 11 mL (**F11**), fraction collected at 12 mL (**F12**), fraction collected at 13 mL (**F13**), fraction collected at 14 mL (**F14**), fraction collected at 15 mL (**F15**).

In contrast, the SEC purification profile of MEG3.4 differed markedly from that of MEG3.3. As shown in **Fig. 10-A**, major, symmetric peak was observed near to fraction collected at 20 mL, which is later than expected for the theoretical molecular mass of MEG3.4. All fractions of interest were analysed by 15 % SDS-PAGE in reduced conditions (with β-mercaptoethanol) to verify MEG3.4 purification and identify the corresponding elution fractions. As shown in **Fig. 10-B**, each fraction displayed a band near the 15 kDa molecular weight marker, consistent with MEG3.4. This distribution suggests that MEG3.4 undergoes partial aggregation during SEC, resulting in a broad elution profile and detection of the protein across multiple fractions, including those eluting later than expected for its theoretical mass (around fraction collected at 20 mL).

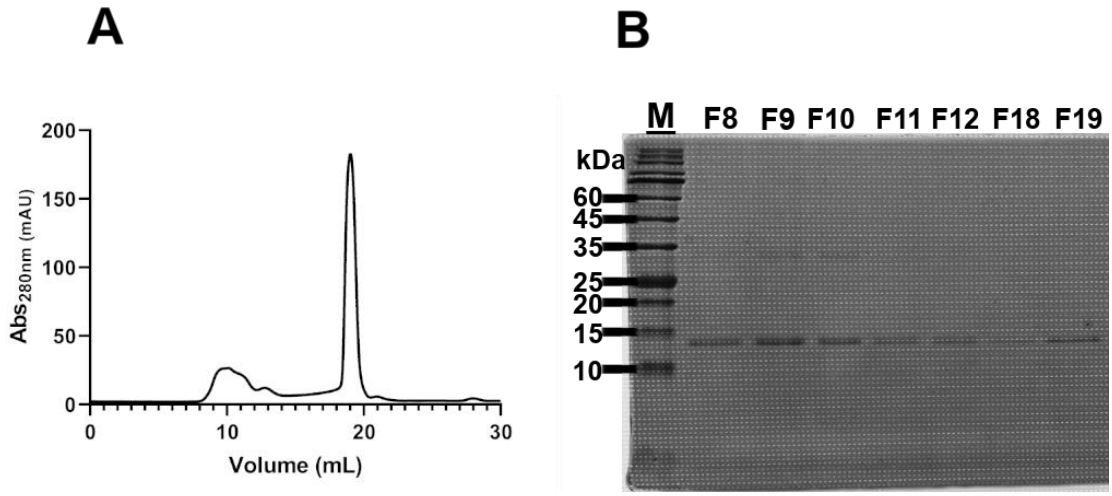

Fig. 10. Size Exclusion Chromatography and SDS-PAGE analysis of MEG3.4 fractions obtained after dialysis protocol. (**A**) Protein profile of MEG3.4 purification by SEC using a Superdex75 Increase 10/300 GL column with an isocratic flow ; fractions/elution volumes were collected to analyzed by (**B**) SDS-PAGE, showing the protein molecular weight marker in kDa (**M**) and the following fractions: fraction collected at 8 mL (**F8**), fraction collected at 9 mL (**F9**), fraction collected at 10 mL (**F10**), fraction collected at 11 mL (**F11**), fraction collected at 12 mL (**F12**), fraction collected at 18 mL (**F18**) and fraction collected at 19 mL (**F19**).

As MEG3.4 protein has a higher expression, but accumulated in inclusion bodies, it was subjected to an alternative refolding strategy. An on-column refolding protocol was performed and optimized by testing different temperatures (25 °C and 18 °C), and flow conditions (gravity and peristaltic pump) **Fig. 11**, this approach resulted in less intense protein bands in elution sample in compared with the conventional denaturing purification process in **Fig. 7**, but with reduced levels of contaminants. The eluted refolded MEG3.4 were subsequently subjected to the SEC purification process.

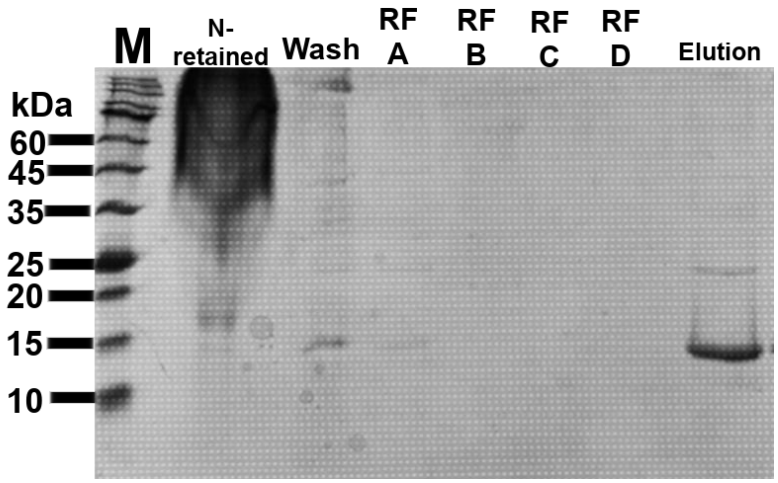

Fig. 11. Purification of MEG3.4 by Nickel Column Affinity in SDS-PAGE using On-column refolding protocol. Protein profile of each step for affinity chromatography purification using the On-column refolding protocol, showing a protein molecular weight marker in kDa (**M**), non-retained (**N- retained**), Refolding buffers **(RF)** and elution.

The new MEG3.4 SEC purification profile from the On-Column refolding process was not better than the MEG3.4 SEC purification by dialysis process. Although protein refolding was achieved in less time than with the dialysis process and with fewer contaminants, the SEC purification profile was unable to separate MEG3.4 from the remaining contaminants. In **Fig. 12-A,** the chromatographic profile is similar to that shown in **Fig. 10-A**. Furthermore, the SDS-PAGE analysis of the collected fractions shows that the protein eluted across multiple fractions, suggesting that the purification process was incomplete. Consequently, MEG3.4 could not be properly characterized.

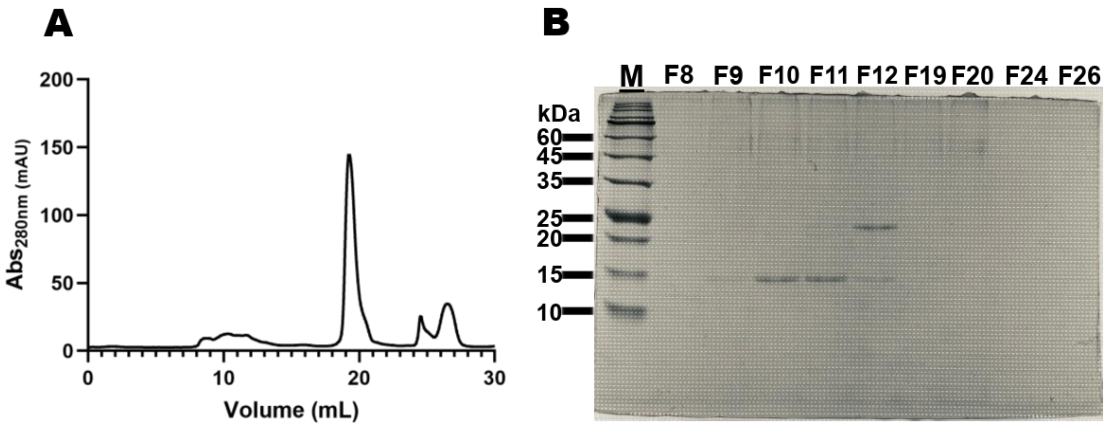

Fig. 12. Size Exclusion Chromatography and SDS-PAGE analysis of MEG3.4 fractions from On-column Refolding protocol. (**A**) Protein profile of MEG3.4 purification by SEC using a Superdex75 Increase 10/300 GL column with an isocratic flow; fractions/elution volumes were collected to analyzed by (**B**) SDS-PAGE, showing the protein molecular weight marker in kDa (**M**) and following fractions: fraction collected at 8 mL (**F8**), fraction collected at 9 mL (**F9**), fraction collected at 10 mL (**F10**), fraction collected at 11 mL (**F11**), fraction collected at 12 mL (**F12**), fraction collected at 19 mL (**F19**), fraction collected at 20 mL (**F20**), fraction collected at 24 mL (**F24**) and fraction collected at 26 mL (**F26**).

To address the persistent aggregation issues, both MEG3.4 and MEG3.3 constructs were transformed by heat shock into a different *E. coli* strain, Rosetta-Gami (DE3) pLysS, a derivative of Origami designed to enhance recombinant expression of cysteine-rich proteins and promote formation of soluble protein. After multiple transformation attempts, recombinant colonies were obtained only for MEG3.4, whereas MEG3.3 colonies could not be obtained.

As shown in **Fig. 13**, a prominent band near the 15 kDa molecular weight marker is observed in the induced sample, corresponding to MEG3.4 expression. A strong band is also present in the pellet samples (inclusion bodies), indicating that although Rosetta-Gami promotes partial solubility, a substantial portion of the protein still accumulates in inclusion bodies.

Finally, the elutions fractions (1 and 2) display prominent bands close to the 15 kDa marker, consistent with the predicted molecular mass of MEG3.4 (15.8 kDa), although some contaminants proteins are still present.

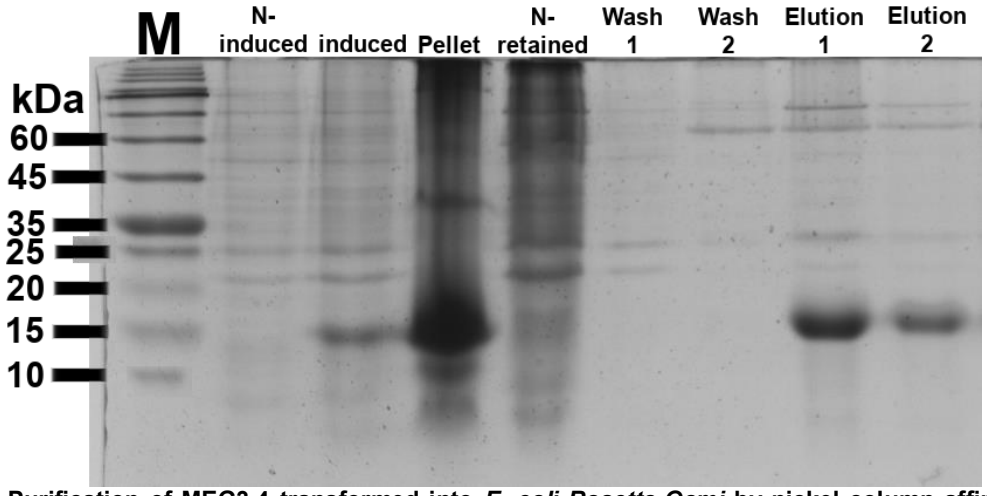

Fig. 13. Purification of MEG3.4 transformed into *E. coli Rosetta-Gami* by nickel column affinity in SDS-PAGE. Protein profile of each step for affinity chromatography purification using soluble fraction, identified with a protein molecular weight marker in kDa (**M**), non-induced (**1**), induced (**2**), pellet (**3**), non-retained (**4**), wash 1 and 2 (**5** and **6**), elutions 1 and 2 (**7** and **8**).

After MEG3.4 soluble protein was obtained from the new Rosetta-Gami2 by affinity chromatography, SEC purification was performed under the same conditions described above. In this case, the SEC purification

profile of MEG3.4 (**Fig. 14-A**) showed clear improvement compared to previous trials, displaying two well-defined and symmetric peaks in fractions collected at 9 mL (**F9**) and 13 mL (**F13**). Subsequent SDS-PAGE analysis (**Fig. 14-B**) confirmed that MEG3.4 protein was successfully purified and eluted at 13 mL (**F13**), as indicated by prominent band above the 10 kDa marker and close to the 15 kDa molecular weight marker. Fractions containing higher-molecular-weight species were discarded.

Despite the successful purification of MEG3.4, the final yield was limited. Eluted fractions were obtained at approximately 5 µM in 25 mM Tris-HCl pH 8.0, 150 mM NaCl and 10% glycerol; and could be concentrated only up to 10 µM using an Amicon Ultra-15 centrifugal filter before it started to aggregate. This limitation was critical for downstream analyses. Consequently, purified MEG3.4 samples were used only for 15% SDS-PAGE in reduced conditions (with β-mercaptoethanol) (as shown before) and circular dichroism (CD) measurements. The use of Tris-HCl buffer is incompatible with DSS-based chemical crosslinking assays due to interference with NHS ester reactions, and the low protein concentration precluded reliable dynamic light scattering (DLS) measurements. In addition, the limited sample volume prevented performing multiple replicates of the $ABTS^{+}$ antioxidant assays.

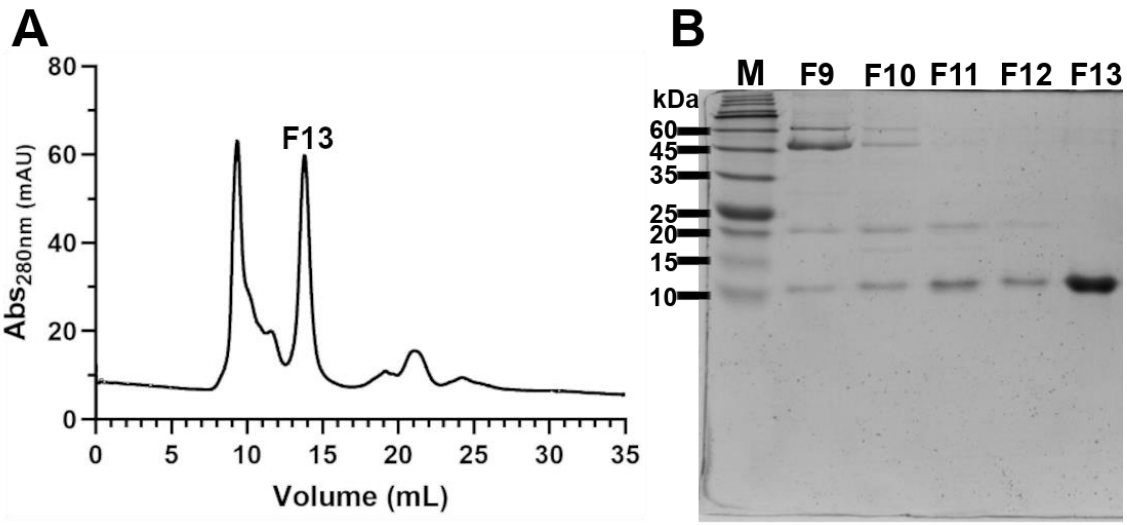

Fig. 14. Size Exclusion Chromatography and SDS-PAGE analysis of MEG3.4 transformed into *E. coli Rosetta-Gami*. (**A**) Protein profile of MEG3.4 purification by SEC using a Superdex75 Increase 10/300 GL column with an isocratic flow; showing the fraction/elution volume of interest (**F13**), fractions/elution volumes were collected to analyzed by (**B**) SDS-PAGE, showing the protein molecular weight marker in kDa (**M**) and the following fractions: fractions collected at 9 mL (**F9**), fraction collected at 10 mL (**F10**), fraction collected at 11 mL (**F11**), fraction collected at 12 mL (**F12**) and fraction collected at 13 mL (**F13**).

4.3. Secondary structure determination

4.3.1. Structural prediction

Given that the primary sequences of MEG3.3 and MEG3.4 remain structurally uncharacterized, we employed AlphaFold2 to generate high confidence *in silico* models. As illustrated in **Fig. 15**, the mature sequences (excluding signal peptides) predominantly adopt organized α-helical bundles. The high predicted local distance difference test (pLDDT) scores (blue/cyan regions) observed in the core of both models provide strong computational support for the stability these folds. These findings suggest that, despite differences in their primary sequences, MEG3.3 and MEG3.4 may share a conserved helical structural framework, although MEG3.4 likely contains less ordered or more dynamic regions that could influence its folding and stability.

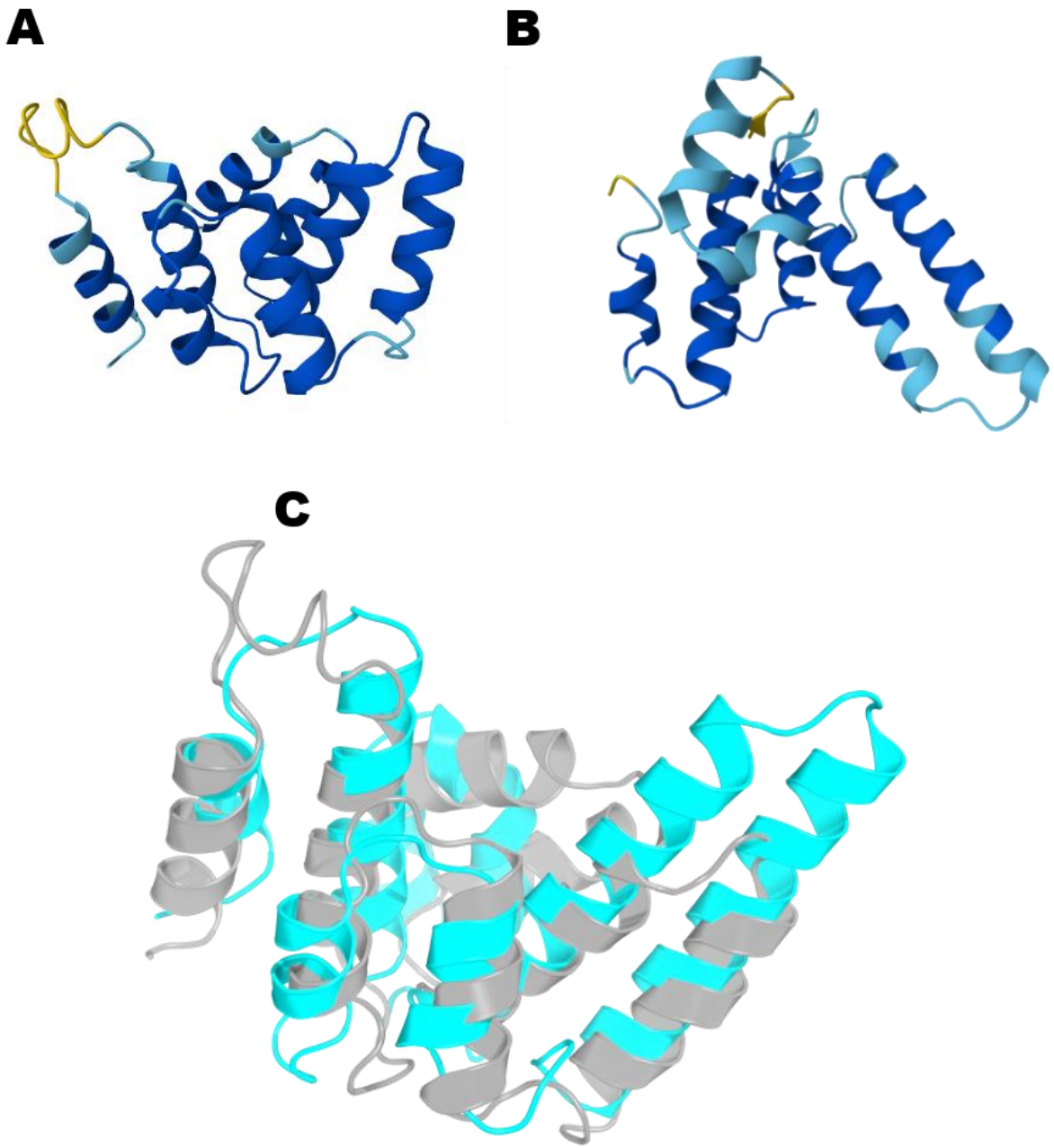

Fig. 15. *In silico* Structural prediction of MEG3.3 and MEG3.4 by AlphaFold3. Structural prediction of (**A**) MEG3.3 and (**B**) MEG3.4 were made by AlphaFold2 using their respective sequences without signal peptide. The reliability of local protein structure prediction is shown in: very high (pLDDT>90, **blue**), confident (80 > pLDDT > 70, **cyan**), ok (70 > pLDDT > 60, **green**), low (60 > pLDDT > 50, **yellow**) and very low (pLDDT < 50, **red**). (**C**) Structural alignment of MEG3.3 (**gray**) and MEG3.4 (**cyan**).

Structural alignment of both MEG proteins (**Fig. 15-C)** revealed partial conservation in the spatial arrangement of four α-helices. However, significant differences in their tertiary structure were observed, specifically within the inter-helical loops regions. In MEG3.4, these loops

appear more extended compared to the more compact loops predicted for MEG3.3. These structural alignments indicates that, although the proteins share a common phylogenetic origin, they have diverged into unique structures. Such structural heterogeneity likely extends to other isoforms within the MEG family, potentially underlying their distinct roles during host infection.

4.3.2. Circular Dichroism

The secondary structure of MEG3.3 and MEG3.4 were experimentally evaluated by far-UV circular dichroism (CD). As shown in **Fig. 16**, the spectral profiles of both proteins are consistent with a predominant α-helical architecture exhibiting the typical double minima at 208 and 222 nm, notably observed for MEG3.3. These results provide experimental support for the structural predictions generated by AlphaFold3 (**Fig. 15**), which suggested a predominantly helical fold for these sequences.

Furthermore, the molar ellipticity at 208 nm being greater than that at 222 nm for MEG3.3 suggests a less stable or more flexible helical structure with increase contributions from disordered or dynamic regions. In contrast, MEG3.4 displays similar magnitudes at both 208 and 222 nm, indicative of a more regular and well-defined α-helical conformation with lower contribution from flexible segments. This structural robustness is significant, as it suggests that the core of the MEG proteins is well organized and may provide an appropriate coordination environment for ion interaction. Collectively, these findings validate the use of AlphaFold3 models as representative frameworks.

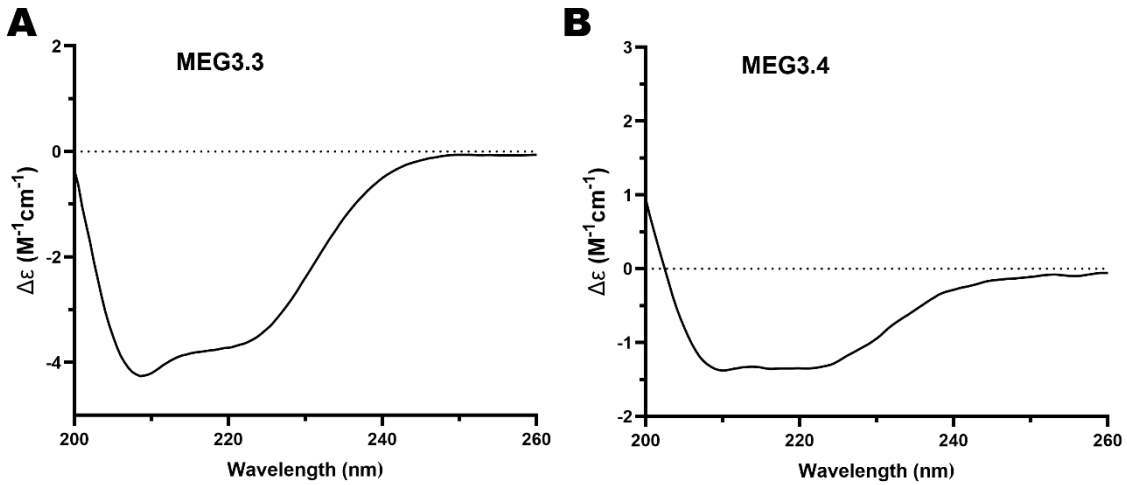

Fig. 16. Circular dichroism analysis of MEG3.3 and MEG3.4. Far-UV spectra of (**A**) MEG3.3 at 20 µM and (**B**) MEG3.4 at 5 µM. Measurements were performed at 20°C in 25 mM Tris-HCl pH 8.0 and 150 mM NaCl. Each curve represents the average of eight consecutive scans.

4.4. Zinc and Copper binding capability

4.4.1. Structural binding prediction

The structural impact of divalent cation coordination on MEG3.3 was evaluated through comparative *in silico* modelling. As illustrated in **Fig. 17-A**, the apo protein is predicted to adopt an organized anti-parallel α-helical architecture. Upon modelling the protein in the presence of either Cu^{2+} (**Fig. 17-B**) or Zn^{2+} (**Fig. 17-C**), the AlphaFold3 algorithm identifies a specific binding pocket where the ions are stabilized by a conserved cluster of coordination residues highlighted in red.

The examination of these models demonstrates that the coordination of both Zn^{2+} and Cu^{2+} is primarily mediated by nitrogen and oxygen-containing side chains, specifically involving a cluster of Histidine (His) and Glutamine (Glu) residues. This finding contrasts with the residues coordination often expected for transition metals in many metallothionein likely protein, which typically rely on Cysteine (Cys) residues to form thiolate-metal bonds. Therefore, for the MEG3.3 prediction, metal ions stabilised by His rings apparently provide the necessary electrical environment for the coordination of these ions.

Structural alignments between the apo and holo forms (**Fig. 17-D** and **E**) demonstrate that the global α-helical scaffold remains highly conserved. The main difference is in the local orientation of these His and Glu side chains, which undergo subtle shifts to satisfy the specific

geometry of the Cu^{2+} and Zn^{2+} ions. These *in silico* models' prediction indicates ions' coordination sites different from our hypothesis of the thiol group of cysteine coordination mechanism, which will also be validated with the chemical crosslinking assays.

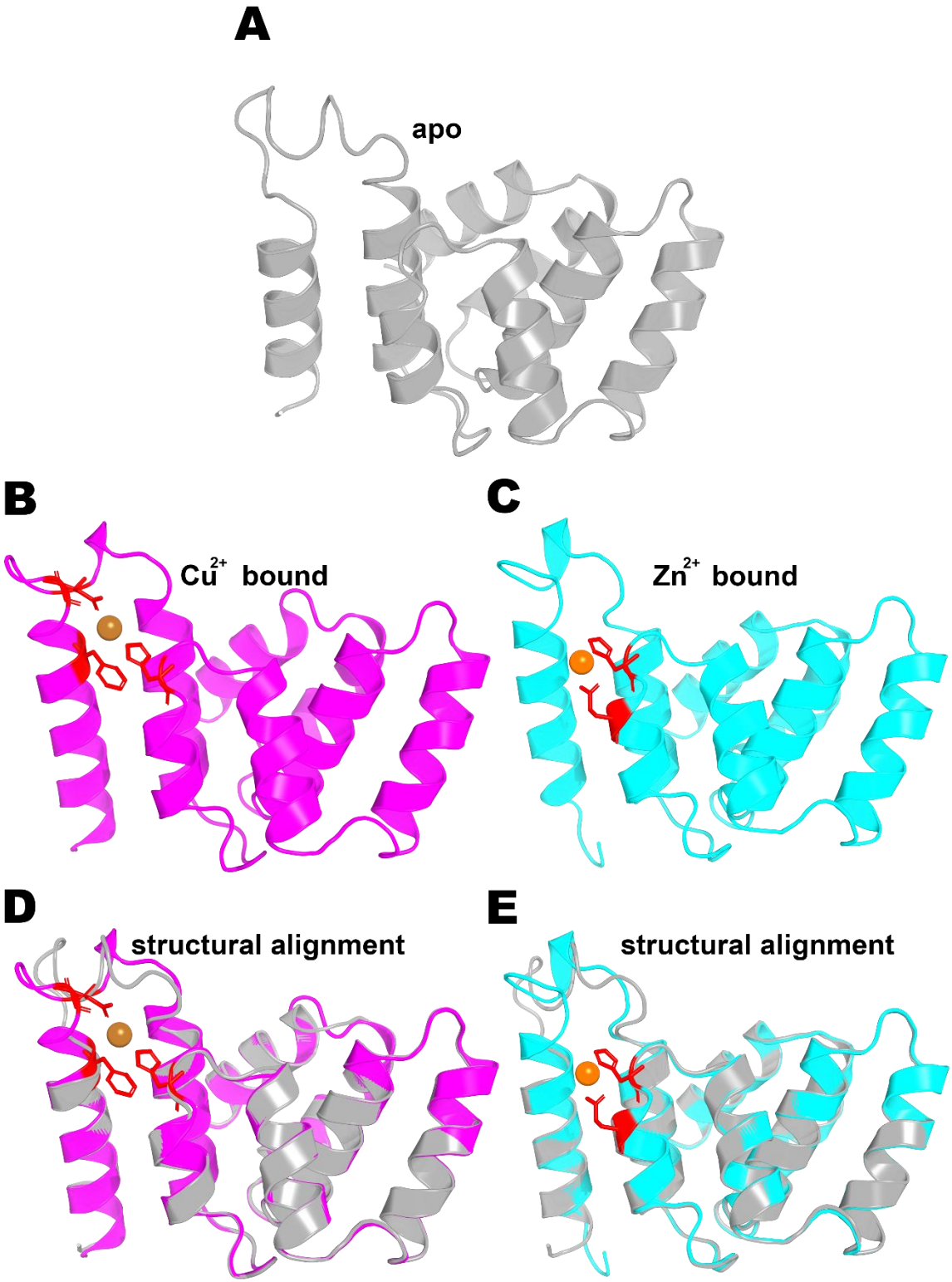

Fig. 17. *In silico* modeling of Metal-Protein Interactions in MEG3.3. AlphaFold3-predicted structures are shown in the (**A**) absence (**apo, gray**), (**B**) presence (**Cu^{2+}-bound**, **magenta**) of a copper ion (**copper sphere**), and (**C**) presence (**Zn^{2+}-bound**, **cyan**) of a zinc ion (**orange sphere**). Residues involved in the coordination site are highlighted in **red**. (**D** and **E**) structural alignment of the apo and holo forms of each respective ion, demonstrating the conformational rearrangement induced by metal binding. Visualization was performed using PyMOL.

The structural architecture of MEG3.4 was modelled to evaluate its folding pattern and potential for metal interaction. As shown in **Fig. 18-A**, the apo protein is predicted to adopt a predominantly α-helical fold, characterized by a series of parallel helices, like MEG3.3. Upon modelling in the presence of Zn^{2+} (**Fig. 18-B**), the protein is shown to stabilize multiple zinc ions within specific coordination pockets.

The coordination interface in MEG3.4 is primarily defined by a cluster of residues highlighted in red, where the spatial arrangement of the side chains allows for the stabilization of the divalent cations. Like the modelling for MEG3.3, the predicted binding sites in MEG3.4 rely extensively on His and Glu residues.

The structural alignment (**Fig. 18-C**) reveals that MEG3.4 did not show significant variation in their tertiary structure. The structural integrity of the helical bundle is maintained, these results suggest that MEG3.4, like MEG3.3, utilizes a robust helical framework to provide a stable environment for metal interaction, but for MEG3.4 those interactions occur in the two parallel largely high α-helical.

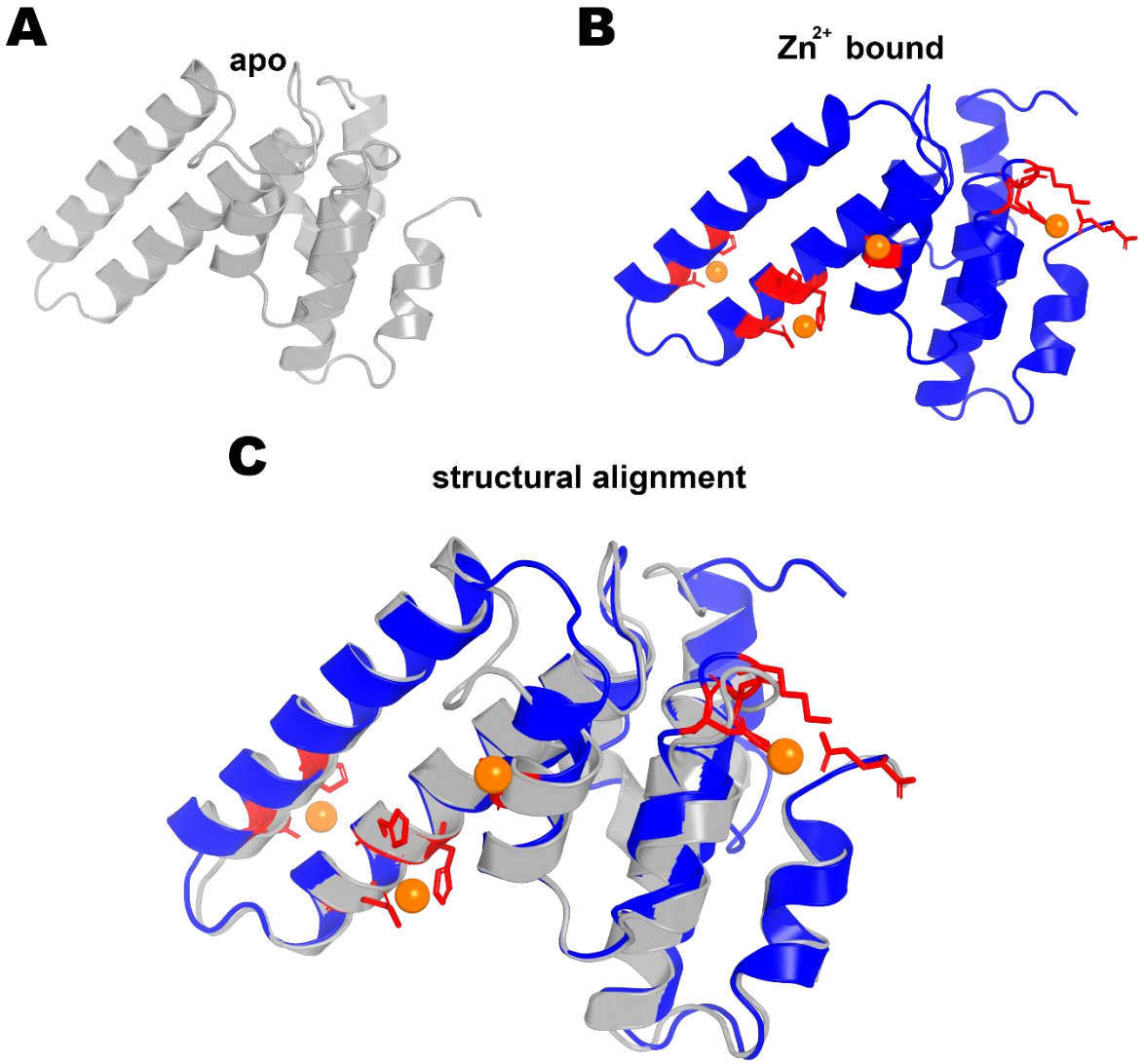

Fig. 18. ***In silico modeling*** **comparison of predicted structural states for MEG3.4 with zinc.** AlphaFold3-predicted structures are shown in the (**A**) absence (**apo, gray**) and (**B**) presence (**Zn^{2+}-bound**, **blue**) of a zinc ion (**orange sphere**). Residues involved in the coordination site are highlighted in **red**. (**C**) structural alignment of the apo and holo forms, demonstrating the conformational rearrangement induced by metal binding. Visualization was performed using PyMOL.

4.4.2. Chemical Crosslinking

To verify MEG3.3 oligomerization induced by these divalent cations, chemical crosslinking assays were performed using purified MEG3.3 at 10 µM in HEPES buffer, using 1 mM DSS as an amine-reactive, non-cleavable cross-linker to stabilize the protein complexes (**Fig. 19** and

Fig. 20). Results shown in **Fig. 19-A**, indicate that MEG3.3 increases its molecular weight after incubation with Zn^{2+} and DSS, starting at a minimum concentration of 100 µM Zn^{2+}, suggesting that

MEG3.3 undergoes oligomerization in the presence of Zn^{2+}. This finding is consistent with the *in silico* models' interactions.

In order to validate the predicted residue interactions mediated by the thiol groups, the same samples were evaluated under reducing conditions in presence of DTT. SDS-PAGE from MEG3.3 analysis of MEG3.3 pre-incubated with DTT (**Fig. 19-B**) showed the same band from apo protein (incubated with DTT and DSS) to protein incubated with DTT and Zn^{2+}, indicating that MEG3.3 protein does not suffer oligomerization when all cysteine residues are reduced. These findings validate the importance of the thiol group in MEG3.3 protein for ions' interactions.

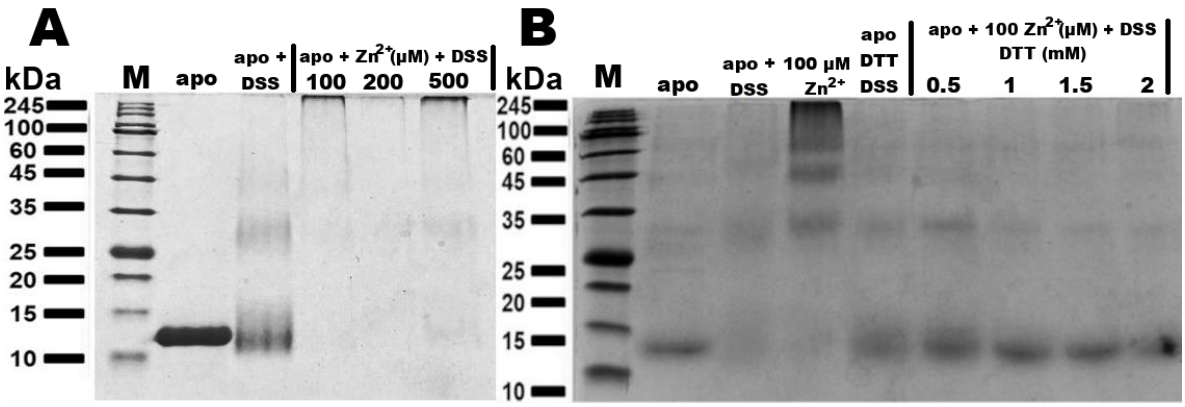

Fig. 19. Chemical Crosslinking and protein analysis of zinc-induced conformational changes in MEG3.3 in SDS-PAGE. (**A**) chemical crosslinking SDS-PAGE of MEG3.3 under Zn^{2+} incubation, showing the protein weight marker size (**M**), apo protein, protein with 1 mM DSS, and incubated with different Zn^{2+} concentrations: 100 µM, 500 µM, and 1 mM. (**B**) chemical crosslinking SDS-PAGE of MEG3.3 under reducing conditions, showing the protein weight marker size (**M**), apo-protein, protein with 1 mM DSS, protein with 100 µM of Zn^{2+}, protein incubated with 1 mM DTT, protein incubated with 100 µM of Zn^{2+} and 0.5 mM DTT, protein incubated with 1 mM DTT, protein incubated with 100 µM of Zn^{2+} and 1.5 mM DTT, protein incubated with 2 mM DTT.

Furthermore, the same chemical crosslinking assays under reducing conditions were also performed for Cu^{2+} interactions (

Fig. 20). Distinct from Zn^{2+} incubation, MEG3.3 samples tend to oligomerize with lower concentrations of Cu^{2+} (50 and 100 µM), forming dimers, while the highest concentration tested resulted in high molecular weight species that did not enter the gel. In both ion incubation conditions, samples pretreated with DTT showed no changes in their apparent molecular mass. Collectively, these findings support the

hypothesis that cysteine thiol groups provide the biochemical framework required for MEG3.3 and MEG3.4, enabling the effective sequestration and coordination of divalent cations such as Zn^{2+} and Cu^{2+}.

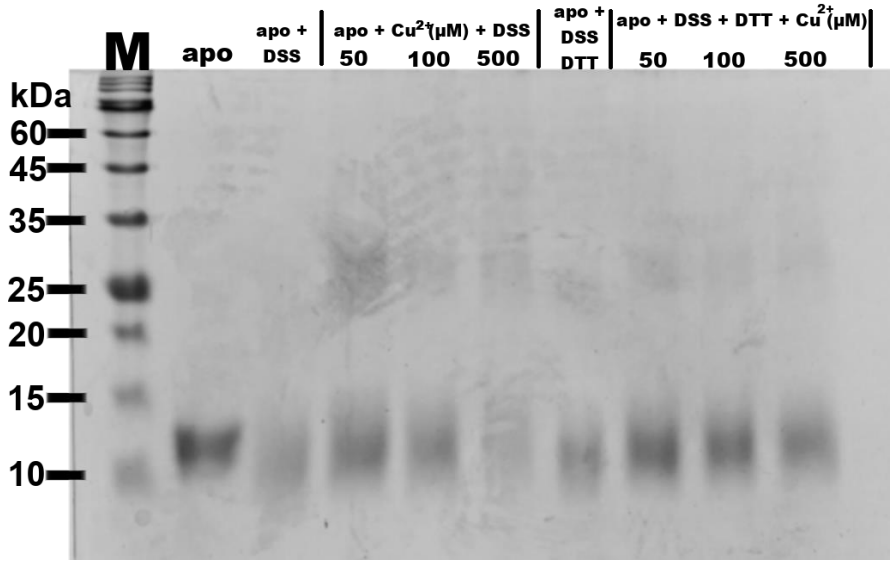

Fig. 20. Chemical Crosslinking and protein analysis of copper-induced conformational changes in MEG3.3 in SDS-PAGE. SDS-PAGE of MEG3.3 crosslinking assay with Cu^{2+}, showing the protein weight marker size **(M),** apo protein, protein incubated with 1 µM DSS as a homobifunctional cross-linker, and incubated with increasing concentrations of Cu^{2+}: 50 µM, 100 µM, and 500 µM; to determine the Cu^{2+} concentration that induced conformational changes; and replicates of those samples (except apo protein) with the addition of 1 mM DTT as a reducing agent.

4.4.3. Particle size with DLS

To further support the ion induced oligomerization results, dynamic light scattering (DLS) assays were performed, in order to determine the hydrodynamic diameter of MEG3.3 protein under different ion concentrations (**Fig. 21**). For Zn^{2+} interactions (**Fig. 21-A**), hydrodynamic diameter increased from 80 µM onwards, and the proteins began to aggregate at 1 mM, corresponding to particles diameter of approximately 100 nm.

Similarly, for Cu^{2+} interactions (**Fig. 21-B**), MEG3.3 exhibited an increase in hydrodynamic diameter from 80 µM Cu^{2+} onwards. However, protein aggregation occurred at 200 µM, earlier than that observed for Zn^{2+}, although it resulted in a similar particle diameter of approximately 100 nm. Control samples containing only buffer with the corresponding ion concentrations were also analysed. These controls confirmed that

neither the buffer nor the ions alone introduced significant interference in the DLS measurements (**Fig. 21**). These findings suggest that MEG3.3 protein increases its hydrodynamic diameter upon binding Zn^{2+} and Cu^{2+}, remaining relatively stable up to approximately 1 mM Zn^{2+} and 200 µM Cu^{2+}, respectively, before the onset of aggregation.

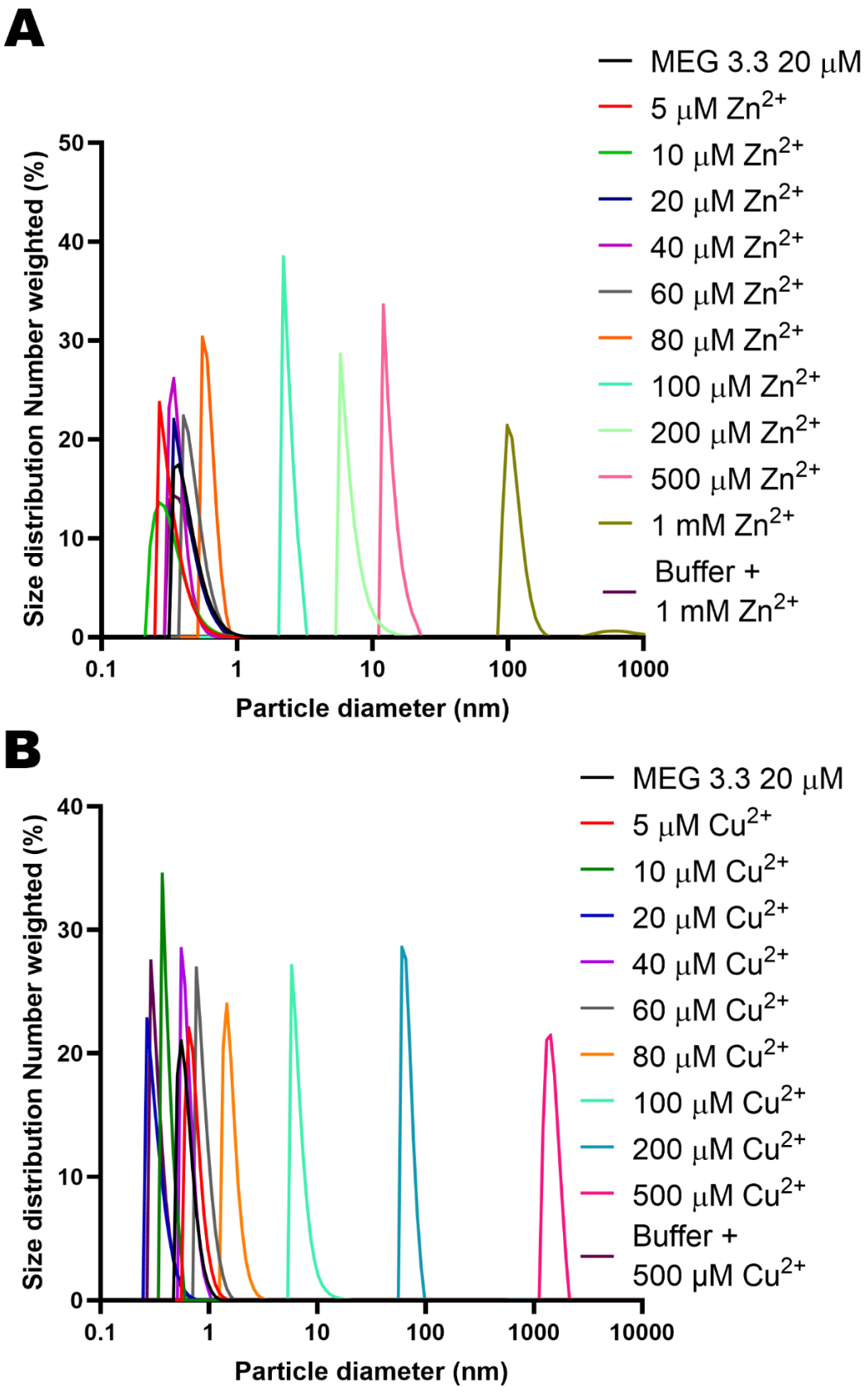

Fig. 21. Impact of Zinc and Copper on the hydrodynamic diameter and oligomerization state of MEG3.3. Particle size distribution was determined by DLS for MEG3.3 (20 μM). (**A**) In the presence of increasing concentrations of Zn^{2+} (0-1 mM), (**B**), and in the presence of increasing concentrations of Cu^{2+} (0-500 μM). Measurements were performed at 25°C in 25 mM Tris-HCl, pH 8.0, and 150 mM NaCl. Each curve represents the average of at least three independent measurements.

4.4.4. Circular Dichroism

Circular dichroism assays were also performed in order to evaluate conformational changes in the secondary structure of each protein (**Fig. 22**). The recorded spectra showed significant variations in the ellipticity of MEG3.3 protein after ion incubation. These changes were more pronounced at 208 nm than 222 nm, with a decrease in signal intensity, suggesting reduced contribution from flexible or disordered regions and increased stabilization of the α-helical structure, thereby enhancing overall protein stability.

For Zn^{2+} samples (**Fig. 22-A**), the CD spectra revealed a marked structural transition at the lowest concentration tested (5 μM) relative to the apo form. This change progressed gradually up to 500 μM, followed by a second pronounced transition at 1 mM, the concentration at which protein aggregation begins. Despite the onset of aggregation, MEG3.3 samples exposed to excess Zn^{2+} partially retained their α-helical structure.

In contrast, for MEG3.3 incubated with for Cu^{2+} (**Fig. 22-B**), the spectral changes were not significant. Although aggregation began at 200 μM, the recorded spectra still indicated retention of the α-helical structure.

For the MEG3.4, due to its low concentration, it was possible to evaluate conformational changes in its secondary structure only in the presence of Zn^{2+} (

Fig. **23**). The MEG3.4 CD spectra showed gradual transition with decreasing signal at both. A more pronounced loss of α-helical signal began at 80 μM Zn^{2+}, with a similar spectral profile maintained at 100 μM, a concentration at which aggregation was observed. These results suggest that the presence of Zn^{2+} induces conformational changes in the secondary structure, with the protein remaining structurally stable up to approximately remaining protein stable up to a concentration of 80 μM.

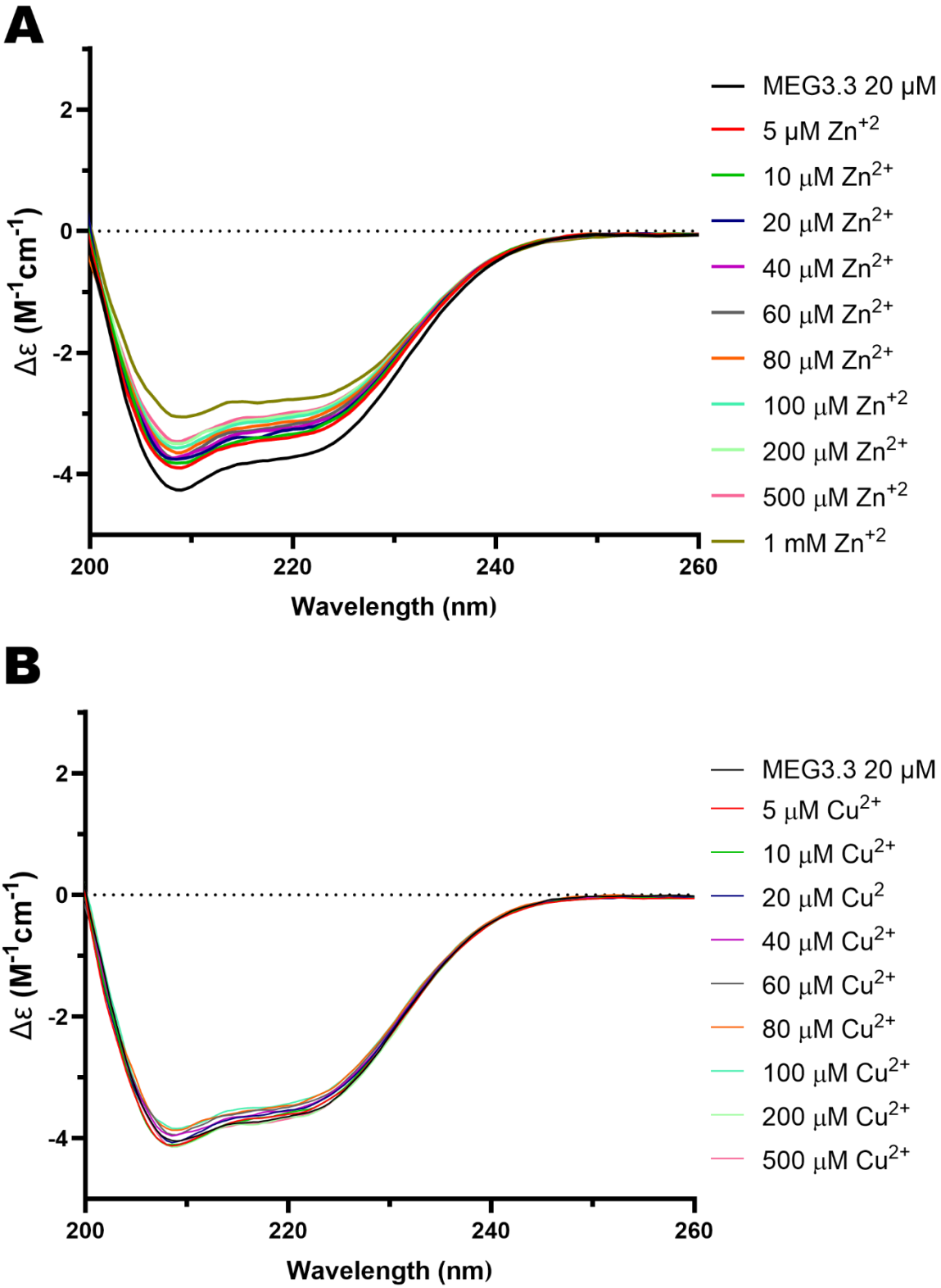

Fig. 22. Analysis of MEG3.3 secondary structure transitions upon zinc and copper titrations. Far-UV circular dichroism spectra were collected for MEG3.3 (20 μM) upon titration with increasing concentrations (0-1 mM) of (**A**) Zn^{2+} and (**B**) Cu^{2+}. All spectra were recorded at 20°C in 25 mM Tris-HCl pH 8.0, and 150 mM NaCl. Each curve represents the meaning of eight consecutive scans.

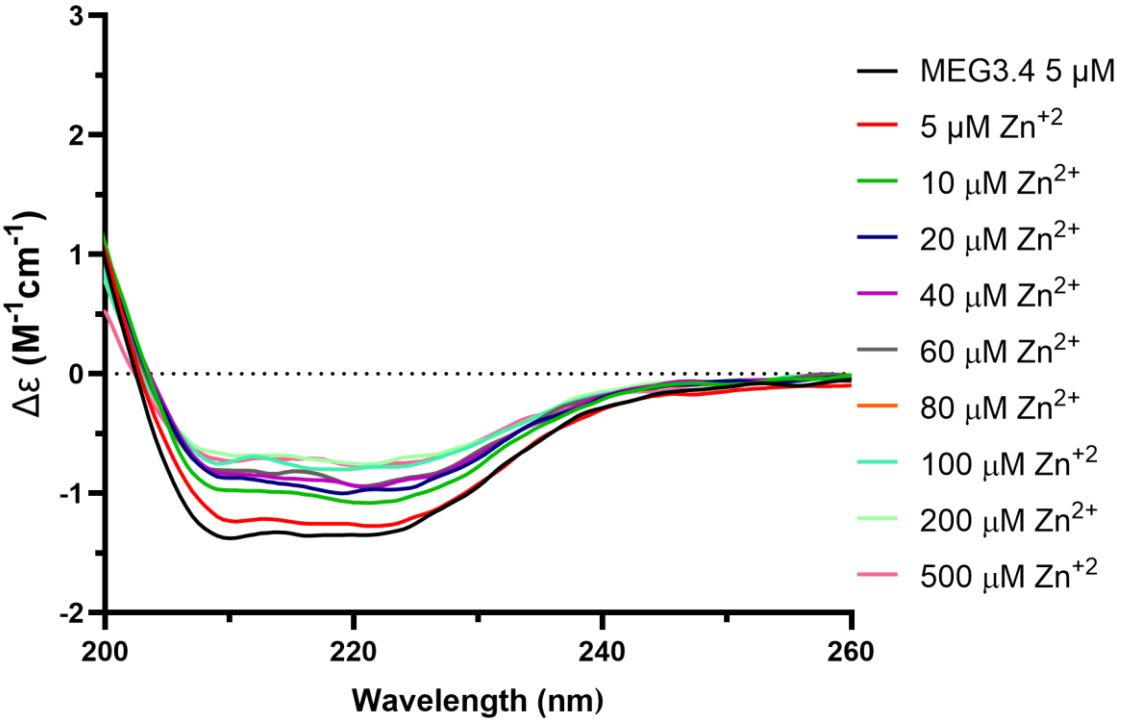

Fig. 23. Analysis of MEG3.4 secondary structure transitions upon zinc titrations. Far-UV circular dichroism spectra were collected for MEG3.4 (5 µM) upon titration with increasing concentrations (0-100 µM) of Zn^{2+}. All spectra were recorded at 20°C in 25 mM Tris-HCl pH 8.0, and 150 mM NaCl. Each curve represents the meaning of eight consecutive scans.

4.5. Antioxidant capability

ABTS^{+} assays were performed to evaluate the radical scavenging activity of MEG3.3 (**Fig. 24**). The results showed that MEG3.3 is capable of scavenging free radicals, exhibiting a minimum activity of 25% inhibition at 1 µM protein and a maximum activity of 96.22% at 10 µM. These findings suggest that MEG3.3 may play a role in oxidative stress-related processes associated with *S. mansoni* parasite survival.

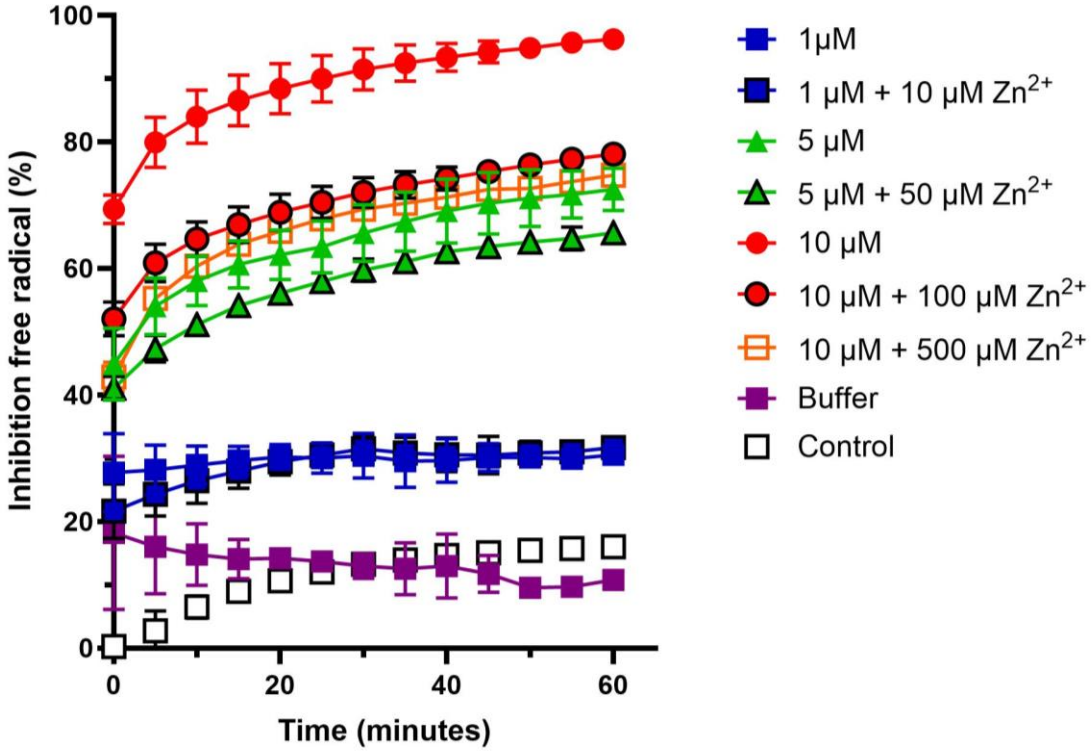

Fig. 24. Radical scavenging activity of MEG3.3. Antioxidant capacity of MEG3.3 was determined by the ABTS assay, measuring the inhibition of free radicals every 5 min over 60 min, and in the presence of increasing Zn^{2+} (10, 50, and 500 μM). Measures were performed at 20°C in 25 mM Tris-HCl pH 8.0, and 150 mM NaCl, using ultrapure water and the same buffer as a negative control.

Additionally, the same assays were performed after incubating MEG3.3 with Zn^{2+}. The results showed an approximate 25% reduction in free radical inhibition following Zn^{2+} incubation, most notably for MEG3.3 at 10 μM. Maintaining the same Zn^{2+}: protein ratio (1:10) also resulted in decreased activity, although the effect was less pronounced than that observed at the highest protein concentration. The estimated IC_{50} for MEG3.3 was 3.07 μM, while for MEG3.3 incubated with Zn^{2+} was 4.21 μM. These findings indicate that Zn^{2+} binding reduces the radical scavenging capacity of MEG3.3, suggesting that Zn^{2+} coordination sites may overlap with residues involved in antioxidant activity, potentially associated with cysteine thiol groups.

5. DISCUSSION

Proteins of the MEG families have attracted considerable interest primarily due to their distinctive sequence features and high expression in key regions of the *S. mansoni* parasite. For instance, MEG3.3 is highly expressed in eggs, whereas MEG3.4 is predominantly expressed in the esophagus. Other members of the MEG family, such as those from the MEG-8 group, have recently been characterized and shown to possess important biochemical functions associated with parasite survival and immune evasion within the human host (Romero et al., 2021; Yadav et al., 2024).

However, unlike MEGs with previously reported functions, members of the MEG-3 family remain poorly characterized, which motivated the present study. In contrast to investigations of the MEG-8 family largely focused on in vivo analyses of parasite survival following gene silencing by RNAi, this works emphasizes the molecular characterization of MEG 3 proteins using biophysical and biochemical approaches. These analyses aim to elucidate the structural and functional behavior of the proteins encoded by the MEG-3 family, particularly in relation to features commonly associated with metallothionein-like proteins.

Sequence analysis revealed a key and distinctive feature of these MEG proteins: the presence of eight pairs of cysteine residues, an unusually high cysteine content for proteins of this size. This characteristic is shared with metallothionein proteins, which, due to their multiple cysteine residues, are often involved in divalent cation binding and oxidative stress-related processes (Sutherland; Stillman, 2011). Despite sharing similar sequences, conserved motifs, and belonging to the same MEG-3 family, the expression and purification behavior of these proteins differed from what was initially expected.

MEG3.3 proved more amenable to expression and purification than MEG3.4. Initial expression in *E. coli* BL21 was successful for both proteins, yielding bands consistent with the expected molecular masses. However, solubility tests indicated that both proteins accumulated in inclusion bodies, necessitating purification under denaturing conditions followed by a refolding step. For MEG3.3, optimization of purification buffers was sufficient to obtain

higher protein concentration in 25 mM Tris-HCl (pH 8.0) and a well-defined peak in the SEC profile (**Fig. 9**).

In contrast, MEG3.4 behave differently. Denaturing and refolding protocols were insufficient to produce highly pure and stable protein, and repeated attempts resulted in aggregation (**Fig. 8**). Indeed, MEG3.4 exhibit behavior typical of cysteine-rich insoluble proteins, often requiring extensive optimization and alternative strategies for successful purification. As reported by Moghadam et al. (2015), such properties are frequently associated with the high cysteine content, since proper disulfide bind formation between cysteine residues depends on an oxidative environment that promotes thiol oxidation.

E. coli BL21, the cytoplasm prevents oxidation, which leads to the erroneous formation of disulfide bonds, and as a result, the protein does not fold correctly, which often exposes hydrophobic residues that cause the protein aggregation and precipitate in the form of inclusion bodies (Kiedzierska et al., 2008; Sørensen; Sperling-Petersen; Mortensen, 2003).

In order to improve the refolding process of MEG3.4, we added an oxidative pair of Cysteine-Cystine reagents in the dialysis buffer, because reduced cysteine can break a malformed disulfide bond, while oxidized cystine provides the potential to form a new one. This dynamic exchange recreates an artificial environment of equilibrium for the protein, which can achieve a lower energy state, which usually related to its native form (Netto et al., 2007). However, this was not enough to improve the refolding process, this may be because some regions tend to fold into each other, forming insoluble aggregates instead of folding correctly. In this regard, Tsumoto et al. (2004) suggests the use of arginine, since by acting weakly with the side chains of the residues, it becomes a shield or spacer that keeps the protein molecules apart. This ultimately reduces the rate of aggregation, giving the protein time to fold correctly; but for MEG3.4 protein was not enough, suggesting that probably the technique of dialysis is not the best.

Accordingly, the refolding technique was shifted to an on-column refolding approach, which yielded improved outcomes for MEG3.4. Although the final protein yield was lower than purification from inclusion bodies, a refolded form of the protein was successfully obtained. This observation is consistent with Li and Huang (2007), who reported that, unlike dialysis, on-

column refolding provides greater control by enabling gradual changes in denaturant condition, thereby minimizing abrupt transitions during folding. In addition, recombinant proteins remain spatially separated through His-tag binding to the resin, which reduces intermolecular interactions between exposed hydrophobic regions during the refolding process. Some studies further suggest that, in this context, the resin can function as a “solid-phase chaperone”, promoting intramolecular folding rather than intermolecular aggregation (Moghadam et al., 2015; Oyeleye et al., 2020). Overall, this approach facilitates adequate interaction with the redox pair, allowing the correct formation of disulfide bonds.

Despite reports by Li and Huang (2007), and Moghadam et al. (2015) describing successful purification of proteins following refolding, MEG3.4 could not be fully isolated after SEC purification. As shown in **Fig. 12**, the chromatographic profile exhibits a broadened peak, with MEG3.4-associatedd bands detected across samples F10 to F12, consistent with the SEC behavior described by Fekete et al. (2014). The atypical MEG3.4 SEC profile could be by different factors, such as the presence of oligomers and soluble aggregations, which broaden the chromatographic profile signal. This behavior was not observed in the earliest eluting peaks, but became evident in sample F12, where an additional higher-molecular-weight band was detected. Such peak broadening is characteristic of polydisperse samples in which multiple oligomeric states coexist in a dynamic equilibrium.

Furthermore, the detection of bands with the identical molecular weight across samples F10 to F12 suggests the occurrence of non-ideal secondary interactions between the protein and the stationary phase. According to Fekete et al. (2014), this behavior stems from electrostatic or hydrophobic affinities that irregularly delay elution, leading to a tailing effect that broadens the absorption peak, and due to the oligomerization process, this may explain the presence of bands corresponding to dimers and other oligomer states of the protein. As indicated by Hall (2018), the elution profile of MEG3.3 shows an intrinsic tendency to form soluble aggregates, despite maintaining its molecular integrity, which is related to the theory of Fekete et al. (2014) , as a polydisperse system characterized by soluble aggregation and secondary interactions with the resin. This behavior, while described as non-ideal, is

frequently encountered during the biophysical analysis of complex recombinant proteins with high structural plasticity.

Since previous refolding strategies did not yield satisfactory purification of MEG3.4, the expression system was changed from *E. coli* BL21 (DE3) to *E. coli* Rosetta-Gami2 (DE3) pLysS, aiming to improve recombinant production of this cysteine-rich protein, as proposed by Kiedzierska et al. (2008). Transformation into this strain resulted in detectable expression of a soluble recombinant fraction-although a substantial proportion of the protein still accumulated in inclusion bodies-representing a key advance toward obtaining MEG3.4 in a soluble state and reducing the need for additional refolding steps.

Consistent with previous studies on cysteine-rich proteins (De O Mello et al., 2014; Kiedzierska et al., 2008), the Rosetta-Gami2 (DE3) pLysS strain, which carries mutations in thioredoxin reductase and glutathione reductase genes, provides a more oxidizing cytoplasmic environment that favors disulfide bond formation. This environment likely contributed to improved folding of MEG3.4, partially preventing complete aggregation into inclusion bodies and enabling subsequent biophysical and biochemical characterization.

Obtaining purified, stable, and isolated MEG proteins was essential for their biophysical characterization. Because the esophagus is critical for parasite feeding and survival, and eggs are central to *S. mansoni* proliferation and maturation, proteins highly expressed in these regions are likely involved in host-parasite interactions, particularly in immune evasion strategies. For this reason, MEG proteins such as MEG3.3 and MEG3.4 remain important targets for molecular characterization.

The metal-induced structural transition observed for MEG3.3 and MEG3.4 show notable parallels with those reported for several well-characterized metalloproteins. Biophysical analyses of recombinant MEG3.3 demonstrated its ability to bind both Zn^{2+} and Cu^{2+}.

Metallothionein protein studies describe them as low molecular weight protein with a rigid secondary structure, often remaining intrinsically disordered in their apo form to allow for structural plasticity during metal cluster formation (Atrian; Capdevila, 2013; Sutherland; Stillman, 2011). In contrast, our Alphafold3 models and CD spectra confirm that MEG3.3 and MEG3.4 adopt helical structures. The structure observed here resembles that of PspA (Ausar

et al., 2017), which maintains stability through a dominant helical colied-coil architecture, and the human KIN protein (Pattaro Júnior et al., 2019), which undergoes specific structural remodeling upon metal binding to satisfy coordination requirements. The persistence of the characteristic double minima at 208 nm and 222 nm, even after metal titration, indicated that-unlike some metallothioneins, which undergo a complete disorder-to-order transition (Atrian; Capdevila, 2013), MEG proteins likely use a pre-formed helical scaffold as a stable framework for metal interaction.

Furthermore, our findings from chemical crosslinking assays, in the absence and presence of reducing agent (DTT), clearly demonstrate that when the protein's cysteines are reduced, the metal-binding effects are not observed. This inhibition of oligomerization by DTT aligns with the fundamental definition of metallothionein, like MT-1 and MT-2 (Atrian; Capdevila, 2013; Yang et al., 2024), which rely on thiol-dependent ligation for Zn^{2+} and Cu^{2+}. In addition, Metallothionein protein are notably devoid of aromatic amino acids (Phe, Tyr and Trp), but MEG3.4 contains Tryptophan and MEG3.3 contains the others aromatic residues. This structural detail, combined with the α-helical structure, suggest that MEGs are a non-typically class of Cys-rich proteins that use aromatic amino acids to stabilize the core while using Cys thiol groups to provide the requisite biochemical framework to sequester metals, a mechanism also reported in specialized domains of the human KIN protein (Pattaro Júnior et al., 2019).

Additionally, a differential sensitivity between those divalent cations was reported. Cu^{2+} induces aggregation at lower concentrations (200 μM) than Zn^{2+} (1 mM) for MEG3.3; this higher sensitivity to Cu^{2+} is similar to the study of SUMO1 (Kaur et al., 2020), where Cu^{2+} was found to have a significantly stronger impact on protein conformation and aggregation kinetics compared to Zn^{2+}. In addition, our DLS and crosslinking data for MEG3.3 confirm a transition from apo-protein to large soluble aggregates. These results reflect the behavior of the human KIN protein (Pattaro Júnior et al., 2019), which undergoes specific oligomerization and structural remodeling upon metal binding to satisfy coordination geometries.

Another important feature is the activity related to oxidative stress. Metallothionein isoforms such as MT-1 have been reported to play protective

roles (Yang et al., 2024), and MT-10 has demonstrated notable antioxidant capacity (Vergani et al., 2007). Similarly, MEG3.3 exhibit strong antioxidant activity, supporting the notion that its cysteine thiol groups are redox-active. The marked reduction in radical scavenging following Zn^{2+} binding suggests competition for these thiol groups, a mechanism comparable to that described for metallothioneins (Atrian; Capdevila, 2013), in which metal coordination and oxidation are coupled processes that regulate protein functional availability and may operate as a redox-sensing mechanism.

These findings may be related to the hostile environment encountered by the parasite within the human host, where *S. mansoni* is exposed to reactive oxygen species (ROS). In this context, MEG proteins may function as multifunctional regulators. Similar to metallothioneins-which have been reported to modulate inflammatory responses and reduce pro-inflammatory cytokines such as IL-6 and TNF-α (Penkowa; Hidalgo, 2001); MEGs may help regulate the local microenvironment by simultaneously neutralizing host-derived radicals and sequestering transitions metals.

6. CONCLUSIONS

In summary, although MEG3.3 and MEG3.4 share conserved motifs and belong to the same MEG family, MEG3.3 proved more amenable to purification than MEG3.4 was sufficiently stable in their stability after purification: refolded MEG3.3 was sufficiently stable to enable the full set of biophysical assays, whereas MEG3.4 required further optimization of the purification process, including for the soluble obtained from Rosetta-Gami2 (DE3) pLysS. Consequently, fewer experiments could be performed for MEG3.4 compared with MEG3.3. Across the purification strategies explored in this work, the combined use of arginine and a redox pair improved refolding efficiency.

Finally, although MEG3.3 shares thiol-dependent metal coordination and antioxidant properties with classical metallothioneins such as MT-1 and MT-10, it retains a pre-folded α-helical architecture that confers greater structural stability during metal titration, a feature more commonly associated with structured regulatory proteins such as SUMO1 or CML14. This dual behavior suggests that MEG proteins may have evolved a specialized structural framework to perform metallothionein-like functions within the extracellular environment of the host.

REFERENCES

ABRAMSON, Josh *et al.* Accurate structure prediction of biomolecular interactions with AlphaFold 3. **Nature 2024 630:8016**, v. 630, n. 8016, p. 493–500, 8 maio 2024.

ACHARYA, Sreemoyee; DA'DARA, Akram A.; SKELLY, Patrick J. Schistosome immunomodulators. **PLoS Pathogens**, v. 17, n. 12, p. e1010064, 1 dez. 2021.

ATRIAN, Sílvia; CAPDEVILA, Mercè. **Metallothionein-protein interactions**. **Biomolecular Concepts**, abr. 2013.

AUSAR, Salvador F. *et al.* Biophysical Characterization and Thermal Stability of Pneumococcal Histidine Triad Protein D in the Presence of Zinc and Manganese. **Journal of Pharmaceutical Sciences**, v. 106, n. 10, p. 2979–2987, 1 out. 2017.

BERRIMAN, Matthew *et al.* The genome of the blood fluke Schistosoma mansoni. **Nature**, v. 460, n. 7253, p. 352–358, 16 jul. 2009.

CHAI, M. *et al.* Transcriptome profiling of lung schistosomula,in vitro cultured schistosomula and adult Schistosoma japonicum. **Cellular and molecular life sciences : CMLS**, v. 63, n. 7–8, p. 919–929, abr. 2006.

CHEEVER, A. W. *et al.* Kinetics of egg production and egg excretion by Schistosoma mansoni and S. japonicum in mice infected with a single pair of worms. **The American journal of tropical medicine and hygiene**, v. 50, n. 3, p. 281–295, 1994.

CHEN, Lin *et al.* Skin-stage schistosomula of Schistosoma mansoni produce an apoptosis-inducing factor that can cause apoptosis of T cells. **Journal of Biological Chemistry**, v. 277, n. 37, p. 34329–34335, 13 set. 2002.

COLLEY, Daniel G. *et al.* Human schistosomiasis. *In*: Elsevier B.V., 2014.

CURWEN, Rachel S. *et al.* Identification of novel proteases and immunomodulators in the secretions of Schistosome cercariae that facilitate host entry. **Molecular and Cellular Proteomics**, v. 5, n. 5, p. 835–844, maio 2006.

DA'DARA, Akram A. *et al.* Schistosome tegumental ecto-apyrase (SmATPDase1) degrades exogenous pro-inflammatory and pro-thrombotic nucleotides. **PeerJ**, v. 2, n. 1, 2014.

DE O MELLO, Érica *et al.* Functional expression and activity of the recombinant antifungal defensin PvD1r from Phaseolus vulgaris L. (common bean) seeds. **BMC Biochemistry 2014 15:1**, v. 15, n. 1, p. 7-, 1 abr. 2014.

DEMARCO, Ricardo *et al.* Protein variation in blood-dwelling schistosome worms generated by differential splicing of micro-exon gene transcripts. **Genome Research**, v. 20, n. 8, p. 1112–1121, ago. 2010.

DOENHOFF, Michael J. *et al.* Resistance of Schistosoma mansoni to praziquantel: is there a problem? **Transactions of The Royal Society of Tropical Medicine and Hygiene**, v. 96, n. 5, p. 465–469, 1 set. 2002.

EL RIDI, Rashika *et al.* Innate immunogenicity and in vitro protective potential of Schistosoma mansoni lung schistosomula excretory--secretory candidate vaccine antigens. **Microbes and infection**, v. 12, n. 10, p. 700–709, set. 2010.

EVERTS, Bart *et al.* Omega-1, a glycoprotein secreted by Schistosoma mansoni eggs, drives Th2 responses. **The Journal of Experimental Medicine**, v. 206, n. 8, p. 1673, 3 ago. 2009.

FEKETE, Szabolcs *et al.* **Theory and practice of size exclusion chromatography for the analysis of protein aggregates**. **Journal of Pharmaceutical and Biomedical Analysis**Elsevier, , 1 dez. 2014.

FIGUEIREDO, Barbara C. *et al.* Schistosomes Enhance Plasminogen Activation: The Role of Tegumental Enolase. **PLoS pathogens**, v. 11, n. 12, 2015.

FOUAD AHMED, S. *et al.* Developmental differences determine larval susceptibility to nitric oxide-mediated killing in a murine model of vaccination against Schistosoma mansoni. **Infection and immunity**, v. 65, n. 1, p. 219–226, 1997.

GOBERT, G. N.; CHAI, M.; MCMANUS, D. P. Biology of the schistosome lung-stage schistosomulum. **Parasitology**, v. 134, n. Pt 4, p. 453–460, abr. 2007.

HALL, Martin. Size Exclusion Chromatography (SEC). *In*: **Biopharmaceutical Processing: Development, Design, and Implementation of Manufacturing Processes**. *[S.l.]*: Elsevier, 2018. p. 421–432.

HAMBROOK, Jacob R.; HANINGTON, Patrick C. **Immune Evasion Strategies of Schistosomes**. **Frontiers in Immunology**Frontiers Media S.A., , 4 fev. 2021.

HOWE, Kevin L. *et al.* WormBase ParaSite − a comprehensive resource for helminth genomics. **Molecular and Biochemical Parasitology**, v. 215, p. 2–10, 1 jul. 2017.

HU, Shaomin *et al.* Molecular cloning and expression of a functional anti-inflammatory protein, Sj16, of Schistosoma japonicum. **International Journal for Parasitology**, v. 39, n. 2, p. 191–200, 15 jan. 2009.

JUMPER, John *et al.* Highly accurate protein structure prediction with AlphaFold. **Nature 2021 596:7873**, v. 596, n. 7873, p. 583–589, 15 jul. 2021.

KATZ, Naftale. **Inquérito Nacional de Prevalência da Esquistossomose mansoni e Geo-helmintoses**. *[S.l.: S.n.]*.

KAUR, Anupreet *et al.* Characterization of Cu2+ and Zn2+ binding sites in SUMO1 and its impact on protein stability. **International Journal of Biological Macromolecules**, v. 151, p. 204–211, 15 maio 2020.

KELLY, Sharon M.; JESS, Thomas J.; PRICE, Nicholas C. How to study proteins by circular dichroism. **Biochimica et Biophysica Acta (BBA) - Proteins and Proteomics**, v. 1751, n. 2, p. 119–139, 10 ago. 2005.

KIEDZIERSKA, Adriana *et al.* Expression, purification and crystallization of cysteine-rich human protein muskelin in Escherichia coli. **Protein Expression and Purification**, v. 60, n. 1, p. 82–88, 1 jul. 2008.

KOKALIARIS, Christos *et al.* Effect of preventive chemotherapy with praziquantel on schistosomiasis among school-aged children in sub-Saharan Africa: a spatiotemporal modelling study. **The Lancet Infectious Diseases**, v. 22, n. 1, p. 136–149, 1 jan. 2022.

LEE, Jayhun; CHONG, Tracy; NEWMARK, Phillip A. The esophageal gland mediates host immune evasion by the human parasite Schistosoma mansoni. **Developmental Biology**, v. 117, n. 32, p. 19299–19309, 2020.

LEONTOVYČ, Adrian *et al.* SmSP2: A serine protease secreted by the blood fluke pathogen Schistosoma mansoni with anti-hemostatic properties. **PLOS Neglected Tropical Diseases**, v. 12, n. 4, p. e0006446, 20 abr. 2018.

LI, Mingcai; HUANG, Dongyang. On-column refolding purification and characterization of recombinant human interferon-λ1 produced in Escherichia coli. **Protein Expression and Purification**, v. 53, n. 1, p. 119–123, 1 maio 2007.

LI, Qin *et al.* Global trends of schistosomiasis burden from 1990 to 2021 across 204 countries and territories: Findings from GBD 2021 study. **Acta Tropica**, v. 261, n. 9, p. 107504, 1 jan. 2025.

LI, Xiao Hong *et al.* Microexon gene transcriptional profiles and evolution provide insights into blood processing by the Schistosoma japonicum esophagus. **PLoS Neglected Tropical Diseases**, v. 12, n. 2, 12 fev. 2018.

LIU, Chang *et al.* Evidence for a protective role of the CX3CL1/ CX3CR1 axis in a model of amyotrophic lateral sclerosis. **Biological Chemistry**, v. 400, n. 5, p. 651–661, 24 abr. 2019.

LU, Hui; WOODBURN, Joanna. Zinc Binding Stabilizes Mitochondrial Tim10 in a Reduced and Import-competent State Kinetically. **Journal of Molecular Biology**, v. 353, n. 4, p. 897–910, 4 nov. 2005.

MARIKOVSKY, M. *et al.* Schistosoma mansoni: killing of transformed schistosomula by the alternative pathway of human complement. **Experimental parasitology**, v. 61, n. 1, p. 86–94, 1986.

MCMANUS, Donald P. *et al.* Schistosomiasis. **Nature Reviews Disease Primers**, v. 4, n. 1, 1 dez. 2018.

MILES, Andrew J.; WALLACE, B. A. CDtoolX, a downloadable software package for processing and analyses of circular dichroism spectroscopic data. **Protein Science**, v. 27, n. 9, p. 1717–1722, 1 set. 2018.

MOGHADAM, Malihe *et al.* Refolding process of cysteine-rich proteins:Chitinase as a model. **Reports of Biochemistry & Molecular Biology**, v. 4, n. 1, p. 19, out. 2015.

MOLEHIN, Adebayo J. **Schistosomiasis vaccine development: Update on human clinical trials**. **Journal of Biomedical Science**BioMed Central Ltd., , 22 jan. 2020.

MORAIS, Suellen B. *et al.* Schistosoma mansoni SmKI-1 serine protease inhibitor binds to elastase and impairs neutrophil function and inflammation. **PLoS pathogens**, v. 14, n. 2, 1 fev. 2018.

NAIDOO, Pragalathan; MKHIZE-KWITSHANA, Zilungile Lynette. **Clustered Regularly Interspaced Short Palindromic Repeats/ CRISPR associated protein 9-mediated editing of Schistosoma mansoni genes: Identifying genes for immunologically potent drug and vaccine development**. **Revista da Sociedade Brasileira de Medicina Tropical**Sociedade Brasileira de Medicina Tropical, , 2022.

NEDVĚDOVÁ, Štěpánka *et al.* Revisiting Schistosoma mansoni Micro-Exon Gene (MEG) Protein Family: A Tour into Conserved Motifs and Annotation. **Biomolecules**, v. 13, n. 9, 1 set. 2023.

NETTO, Luis Eduardo Soares *et al.* Reactive cysteine in proteins: Protein folding, antioxidant defense, redox signaling and more. **Comparative Biochemistry and Physiology Part C: Toxicology & Pharmacology**, v. 146, n. 1–2, p. 180–193, 1 jul. 2007.

ORCIA, Débora *et al.* Interaction of an esophageal MEG protein from schistosomes with a human S100 protein involved in inflammatory response. **Biochimica et Biophysica Acta - General Subjects**, v. 1861, n. 1, p. 3490–3497, 1 jan. 2017.

OYELEYE, Ayokunmi Omolola *et al.* Effective refolding of a cysteine rich glycoside hydrolase family 19 recombinant chitinase from Streptomyces griseus by reverse dilution and affinity chromatography. **PLOS ONE**, v. 15, n. 10, p. e0241074, 1 out. 2020.

PATTARO JÚNIOR, José Renato *et al.* Biophysical characterization and molecular phylogeny of human KIN protein. **European Biophysics Journal**, v. 48, n. 7, p. 645–657, 1 out. 2019.

PEARCE, Edward J. Priming of the immune response by schistosome eggs. **Parasite Immunology**, v. 27, n. 7–8, p. 265–270, jul. 2005.

PENKOWA, Milena; HIDALGO, Juan. Metallothionein Treatment Reduces Proinflammatory Cytokines IL-6 and TNF-α and Apoptotic Cell Death during Experimental Autoimmune Encephalomyelitis (EAE). **Experimental Neurology**, v. 170, n. 1, p. 1–14, 1 jul. 2001.

RE, Roberta *et al.* Antioxidant activity applying an improved ABTS radical cation decolorization assay. **Free radical biology & medicine**, v. 26, n. 9–10, p. 1231–1237, maio 1999.

ROMERO, Aracely A. *et al.* The Schistosoma mansoni nuclear receptor FTZ-F1 maintains esophageal gland function via transcriptional regulation of meg-8.3. **PLOS Pathogens**, v. 17, n. 12, p. e1010140, 1 dez. 2021.

SALZET, M.; CAPRON, A.; STEFANO, G. B. Molecular crosstalk in host-parasite relationships: Schistosome- and leech-host interactions. **Parasitology Today**, v. 16, n. 12, p. 536–540, 1 dez. 2000.

SCHRAMM, Gabriele *et al.* Cutting edge: IPSE/alpha-1, a glycoprotein from Schistosoma mansoni eggs, induces IgE-dependent, antigen-independent IL-4 production by murine basophils in vivo. **Journal of immunology (Baltimore, Md. : 1950)**, v. 178, n. 10, p. 6023–6027, 15 maio 2007.

SKRZYNIARZ, Kinga *et al.* Molecular mechanism of action of imidazolium carbosilane dendrimers on the outer bacterial membrane – From membrane damage to permeability to antimicrobial endolysin. **Journal of Colloid and Interface Science**, v. 665, p. 814–824, 1 jul. 2024.

SMITH, Philip *et al.* Schistosoma mansoni secretes a chemokine binding protein with antiinflammatory activity. **The Journal of experimental medicine**, v. 202, n. 10, p. 1319–1325, 21 nov. 2005.

SØRENSEN, Hans Peter; SPERLING-PETERSEN, Hans Uffe; MORTENSEN, Kim Kusk. Dialysis strategies for protein refolding: preparative streptavidin production. **Protein Expression and Purification**, v. 31, n. 1, p. 149–154, 1 set. 2003.

ŠTĚPÁNKA NEDVĚDOVÁ. **Structural and interaction study of MEG family proteins and their role in liver fibrosis onset**. thesis—Prague: CZECH UNIVERSITY OF LIFE SCIENCES PRAGUE, 2023.

SUTHERLAND, Duncan E. K.; STILLMAN, Martin J. The “magic numbers” of metallothionein. **Metallomics**, v. 3, n. 5, p. 444–463, 1 maio 2011.

SUTTIPRAPA, Sutas; RINALDI, Gabriel; BRINDLEY, Paul J. **Genetic manipulation of schistosomes - Progress with integration competent vectors**. **Parasitology**, abr. 2012.

TORPIER, G.; CAPRON, A.; OUAISSI, M. A. Receptor for IgG(Fc) and human beta2-microglobulin on S. mansoni schistosomula. **Nature**, v. 278, n. 5703, p. 447–449, 1979.

TSUMOTO, Kouhei *et al.* Role of arginine in protein refolding, solubilization, and purification. **Biotechnology Progress**, v. 20, n. 5, p. 1301–1308, 1 jan. 2004.

VERGANI, Laura *et al.* Molecular characterization and function analysis of MT-10 and MT-20 metallothionein isoforms from Mytilus galloprovincialis. **Archives of Biochemistry and Biophysics**, v. 465, n. 1, p. 247–253, 1 set. 2007.

VIEIRA, Paulo *et al.* Latent Schistosomiasis in Portuguese Soldiers. **Military Medicine**, v. 172, n. 2, p. 144–146, 1 fev. 2007.

WANG, Qiang; DA'DARA, Akram A.; SKELLY, Patrick J. The human blood parasite Schistosoma mansoni expresses extracellular tegumental calpains that cleave the blood clotting protein fibronectin. **Scientific reports**, v. 7, n. 1, 1 dez. 2017.

WHO GUIDELINE on control and elimination of human schistosomiasis. . *[S.l.: S.n.]*.

WILSON, R. Alan *et al.* The Schistosome Esophagus Is a 'Hotspot' for Microexon and Lysosomal Hydrolase Gene Expression: Implications for Blood Processing. **PLOS Neglected Tropical Diseases**, v. 9, n. 12, p. e0004272, 7 dez. 2015.

YADAV, Pallavi *et al.* Schistosome esophageal gland factor MEG-8.2 drives host cell lysis and interacts with host immune proteins. **bioRxiv : the preprint server for biology**, 15 nov. 2024.

YANG, Ruoqiu *et al.* **Metallothionein: A Comprehensive Review of Its Classification, Structure, Biological Functions, and Applications**. **Antioxidants**Multidisciplinary Digital Publishing Institute (MDPI), , 1 jul. 2024.

YOU, Hong *et al.* CRISPR/Cas9-mediated genome editing of Schistosoma mansoni acetylcholinesterase. **The FASEB Journal**, v. 35, n. 1, p. e21205, 1 jan. 2021.